

Modeling, Simulation and Analysis of a Clinical PET System With

GATE Software and Monte Carlo Model

by

Sowmiya Raj Thirumalai

A Thesis Presented in Fulfillment
of the Requirements for the Degree
Master of Science

Approved April 2020 by the
Graduate Supervisory Committee:

Dragica Vasileska, Chair
Amirhossein Goldan
Stephen Goodnick

ARIZONA STATE UNIVERSITY

May 2020

ABSTRACT

Positron emission tomography (PET) is a non-invasive molecular imaging technique widely used for the quantification of physiological and biochemical processes in preclinical and clinical research. Due to its fundamental role in the health care system, there is a constant need for improvement and optimization of its scanner systems and protocols leading to a dedicated active area of research for PET. (Geant4 Application for Tomographic Emission (GATE) is a simulation platform designed to model and analyze a medical device. Monte Carlo simulations are essential tools to assist in optimizing the data acquisition protocols or in evaluating the correction methods for improved image quantification. Using GATE along with Customizable and Advanced Software for Tomographic Reconstruction (CASToR), provides a link to reconstruct the images.

The goal of this thesis is to learn PET systems that involve Monte Carlo methods, GATE software, CASToR software to model, simulate and analyze PET systems using three clinical PET systems as a template. Fluorine-18 radioisotope source is used to perform measurements on the modeled PET systems. Parameters such as scatter-fraction, random-fraction, sensitivity, count rate performance, signal to noise ratio (SNR), and time of flight (ToF) are analyzed to determine the performance of the systems. Also, the simulated data are provided as input to CASToR software and Amide's a Medical Image Data Examiner (AMIDE) tool to obtain the reconstructed images which are used to analyze the reconstruction capability of the simulated models. The Biograph Vision PET model has high sensitivity (11.159 cps/MBq) and SNR (12.556) while the Ultra-High Resolution (UHR) PET model has high resolution of the reconstructed image.

DEDICATION

Dedicated to my mother, Raji Dorairaj,
my brother, Sai Raj
and my close friend, Rakesh Natarajan
for their love, understanding and support

ACKNOWLEDGEMENTS

First and most of all, I would like to express my sincere gratitude to Dr. Dragica Vasileska and Dr. Amirhossein Goldan for their expertise, assistance, guidance and support throughout the process of my research and thesis work. I would also like to express a special thanks to Dr. Dragica Vasileska for this opportunity, encouraging and mentoring me throughout the work. I would also like to express my gratitude to Dr. Stephen Goodnick for his support and suggestions.

I would like to extend my thanks to all my friends who helped, guided and supported me throughout the thesis work, especially Abdul Rawoof Shaik (ASU), Xinjie Cao (SBU), Viswanathan Naveen Kumar (ASU) and Chi-Yin Cheng (ASU).

TABLE OF CONTENTS

	Page
LIST OF TABLES	vii
LIST OF FIGURES	ix
LIST OF ABBREVIATIONS.....	xiv
GLOSSARY	xvii
CHAPTER	
1 INTRODUCTION	1
2 POSITRON EMISSION TOMOGRAPHY	3
2.1 Introduction	3
2.2 History.....	3
2.3 Radiotracers Used	4
2.4 Operation.....	6
2.5 PET Scanner	7
2.6 Time-of-Flight (TOF).....	10
2.7 Depth of Interaction (DOI).....	11
2.8 Medical Applications	12
2.9 Safety Concerns	13
2.10 Limitations	13

CHAPTER	Page
3 BACKGROUND OF MODELING AND SIMULATION OF PET SYSTEMS ...	14
3.1 Introduction	14
3.2 Monte Carlo Simulation	15
3.3 SimSET	16
3.4 PETSIM	17
3.5 EIDOLON	18
3.6 Geant4	18
3.7 GATE (Geant4 Application for Tomographic Emission)	19
3.8 ROOT	29
3.9 CASToR	29
3.10 AMIDE (Amide's a Medical Image Data Examiner)	31
4 MODELING AND SIMULATION OF PET SYSTEMS	32
4.1 World volume	34
4.2 PET System Selection	35
4.3 Defining Scanner Geometry	38
4.4 Defining Phantom geometry	54
4.5 Setting-up the Physics Processes	58
4.6 Initialization	59

CHAPTER	Page
4.7 Digitizer Definition	59
4.8 Source Definition	60
4.9 Defining Data Output.....	61
4.10 Starting an Acquisition and Running the Simulation.....	61
5 SIMULATION RESULTS AND PARAMETERS	62
5.1 Sensitivity.....	62
5.2 Noise Equivalent Count Rate (NECR) and Signal-to-Noise Ratio (SNR) ...	66
5.3 True Fraction and Random Fraction	69
5.4 Scatter Fraction	72
5.5 Time Resolution and ToF Gain.....	73
5.6 Image Quality and Reconstruction Using CASToR	80
6 CONCLUSION AND FUTURE WORK	85
6.1 Conclusion.....	85
6.2 Future Prospects	88
REFERENCES	89

LIST OF TABLES

Table	Page
1. Positron-Emitting Radiotracers	5
2. β^+ -Emitters and Their Energy Characteristics	5
3. Properties of Common Scintillators Used in PET Applications.....	9
4. Design Specifications of UHR, HRRT and Biograph Vision PET Scanners	33
5. Sensitivity for Biograph Vision PET System	63
6. Sensitivity for HRRT PET System	64
7. Sensitivity for UHR PET System	65
8. NECR for Biograph Vision PET System.....	67
9. NECR for HRRT PET System.....	67
10. NECR for UHR PET System.....	68
11. True Fraction and Random Fraction for Biograph Vision PET System.....	70
12. True Fraction and Random Fraction for HRRT PET System.....	70
13. True Fraction and Random Fraction for UHR PET System.....	70
14. Scatter Fraction for Biograph Vision, HRRT and UHR PET Systems.....	73
15. NECR and SNR With ToF for Biograph Vision PET System.....	74

Table	Page
16. NECR and SNR With ToF for HRRT PET System	74
17. NECR and SNR With ToF for UHR PET System.....	75
18. Scatter Fraction With ToF for Biograph Vision PET System	77
19. Scatter Fraction With ToF for HRRT PET System	78
20. Scatter Fraction With ToF for UHR PET System	78
21. ToF Gain and SNR Gain for $D = 40$ cm	80
22. Image Quality Analysis for Biograph Vision PET System	80
23. Image Quality Analysis for HRRT PET System	81
24. Image Quality Analysis for UHR PET System.....	81

LIST OF FIGURES

Figure	Page
1. Positron Decay – Proton Converted to a Neutron, a Positron and a Neutrino.....	7
2. Positron Annihilation Reaction	7
3. Schematic View of Detector Block With PMT Example	8
4. Schematic Views of PET Acquisition Process	9
5. Event Localization Using ToF Technique	11
6. Block Diagram of the Various Modules of SimSET	17
7. General Structure of GATE	20
8. Steps for Simulation	23
9. Flowchart for Digitizer - Signal Processing	26
10. Block Diagram for Digitizer	26
11. Depiction of the Different Coincidence Events	27
12 a. Code for World Volume.....	34
12 b. Simulated World Volume	34
13 a. Code for Cylindrical PET Volume for UHR	35
13 b. Simulated Cylindrical PET Volume for UHR	35

Figure	Page
13 c. Code for Cylindrical PET Volume for HRRT	36
13 d. Simulated Cylindrical PET Volume for HRRT	36
13 e. Code for Cylindrical PET Volume for Biograph Vision	37
13 f. Simulated Cylindrical PET Volume for Biograph Vision	37
14 a. Code for Rsector Level / Volume for UHR	39
14 b. Simulated Rsector Level / Volume for UHR	39
14 c. Code for Rsector Level / Volume for HRRT	40
14 d. Simulated Rsector Level / Volume for HRRT	40
14 e. Code for Rsector Level / Volume for Biograph Vision	41
14 f. Simulated Rsector Level / Volume for Biograph Vision	41
15 a. Code for Block Level / Volume for UHR	42
15 b. Simulated Block Level / Volume for UHR	42
15 c. Code for Block Level / Volume for Biograph Vision	43
15 d. Simulated Block Level / Volume for Biograph Vision	43
16 a. Code for Crystal Level / Volume for UHR	44
16 b. Simulated Crystal Level / Volume for UHR	44

Figure	Page
16 c. Code for Crystal Level / Volume for HRRT	45
16 d. Simulated Crystal Level / Volume for HRRT	45
16 e. Code for Crystal Level / Volume for Biograph Vision	46
16 f. Simulated Crystal Level / Volume for Biograph Vision	46
17 a. Code for Layer Level / Volume for UHR	47
17 b. Simulated Layer Level / Volume for UHR	47
17 c. Code for Layer Level / Volume for HRRT	48
17 d. Simulated Layer Level / Volume for HRRT	48
17 e. Code for Layer Level / Volume for Biograph Vision	49
17 f. Simulated Layer Level / Volume for Biograph Vision	49
18 a. Code for Crystal Level Repeater for UHR.....	50
18 b. Simulated Crystal Level Repeater for UHR	50
18 c. Code for Crystal Level Repeater for HRRT	51
18 d. Simulated Crystal Level Repeater for HRRT	51
18 e. Code for Crystal Level Repeater for Biograph Vision	51
18 f. Simulated Crystal Level Repeater for Biograph Vision	51

Figure	Page
19 a. Code for Block Level Repeater for UHR	52
19 b. Simulated Block Level Repeater for UHR	52
19 c. Code for Block Level Repeater for Biograph Vision	52
19 d. Simulated Block Level Repeater for Biograph Vision	52
20 a. Code for Rsector Level Repeater for UHR	53
20 b. Simulated Rsector Level Repeater for UHR.....	53
20 c. Code for Rsector Level Repeater for HRRT	53
20 d. Simulated Rsector Level Repeater for HRRT	53
20 e. Code for Rsector Level Repeater for Biograph Vision	54
20 f. Simulated Rsector Level Repeater for Biograph Vision	54
21. Simulated NEMA 4 Cube Phantom	56
22. Simulated NEMA 2 Cylindrical Phantom	56
23. Simulated NEMA 2 IEC Phantom (Shown in Different Angles).....	57
24. Simulated NEMA 4 IQ Phantom	57
25. Simulated Voxelized Brain Phantom	57
26. Code for Initialization	59

Figure	Page
27. Sensitivity Profile for Biograph Vision, HRRT and UHR PET Systems	66
28. NECR Performance for Biograph Vision, HRRT and UHR PET Systems	68
29. SNR vs Source Activity for Biograph Vision, HRRT and UHR PET Systems	69
30. True Fraction for Biograph Vision, HRRT and UHR PET Systems	71
31. Random Fraction for Biograph Vision, HRRT and UHR PET Systems	72
32. NECR vs Time Resolution for Biograph Vision, HRRT and UHR PET Systems	75
33. SNR vs Time Resolution for Biograph Vision, HRRT and UHR PET Systems.....	76
34. TF vs Time Resolution for Biograph Vision, HRRT and UHR PET Systems	76
35. RF vs Time Resolution for Biograph Vision, HRRT and UHR PET Systems	77
36. SF vs Time Resolution for Biograph Vision, HRRT and UHR PET Systems	78
37. Reconstructed Image (Transverse, Coronal, Sagittal) for Biograph Vision PET	83
38. Reconstructed Image (Transverse, Coronal, Sagittal) for HRRT PET.....	83
39. Reconstructed Image (Transverse, Coronal, Sagittal) for UHR PET	83
40. Pixelated Image (Transverse, Coronal, Sagittal) for Biograph Vision PET.....	84
41. Pixelated Image (Transverse, Coronal, Sagittal) for HRRT PET.....	84
42. Pixelated Image (Transverse, Coronal, Sagittal) for UHR PET	84

LIST OF ABBREVIATIONS

2D – Two Dimensional

3D – Three Dimensional

AMIDE - Amide's a Medical Image Data Examiner

APD – Avalanche Photo Diode

API - Application Programming Interface

ASCII - American Standard Code for Information Interchange

BGO - Bismuth germanium oxide crystal

Bq - Becquerel

CASToR - Customizable and Advanced Software for Tomographic Reconstruction

Ce - Cerium

CERN - European Organization for Nuclear Research (Conseil Européen pour la Recherche)

cps – counts per second

CPU - Central Processing Unit

CT - Computed Tomography

CTR - Coincidence Time Resolution

C11 – Carbon 11 radioisotope

DOI – Depth Of Interaction

EPFL - Electromagnetic Compatibility Laboratory (Ecole Polytechnique Fédérale de Lausanne)

eV – Electron Volts

fMRI - functional Magnetic Resonance Imaging

FOV – Field Of View

FWHM – Full Width at Half Maximum

F18 – Fluorine 18 radioisotope

GATE - Geant4 Application for Tomographic Emission

Geant4 – Geometry and Tracking

GPS - General Particle Source

GRID - Graphic Retrieval and Information Display

HRRT - High-Resolution Research Tomograph

IEC - International Electrotechnical Commission

I/O – Input / Output

IQ – Image Quality (phantom)

LaBr - Lanthanum (III) Bromide

LMF - List Mode Format

LOR – Line Of Response

LSO - Lutetium oxyorthosilicate crystal

LuAP - Lutetium Aluminium Perovskite crystal

LYSO - Lutetium-yttrium oxyorthosilicate crystal

MLEM - Maximum-Likelihood Expectation-Maximization algorithm

MLTR - Maximum-Likelihood Transmission algorithm

MRI - Magnetic Resonance Imaging

NaI:Tl - Sodium iodide activated with thallium

NECR - Noise-equivalent count rate

NEMA - National Electrical Manufacturers Association

N13 – Nitrogen 13 radioisotope

OpenGL - Open Graphics Library

O15 – Oxygen 15 radioisotope

PET - Positron Emission Tomography

PETSIM – Positron Emission Tomography Simulator

pH - potential hydrogen (relative acidity scale)

PMT - Photomultiplier tubes

PSF – Point spread function

PVE – Partial Volume Effect

ROI - Region of Interests

RF – Random Fraction

SF – Scatter Fraction

SimSET - Simulation System for Emission Tomography

SiPM - Silicon Photomultiplier

SNR – Signal to Noise Ratio

SPECT - Single Photon Emission Computed Tomography

STIR - Software for Tomographic Image Reconstruction

TF – True Fraction

ToF – Time of Flight

UHR – Ultra High Resolution

GLOSSARY

Detector response: a record of when a particle passes through the volume of a detector and approximating how a real detector would respond

Gamma rays: an electromagnetic radiation of extremely short wavelength emitted during radioactive decay

Geometry: an analysis of the physical layout of the experiment which includes crystals, detectors, absorbers, etc., and the effect of this layout on the path of particles in the experiment

Glucose: a simple sugar which is an important source of energy for the body and the only source of energy for the brain

Histogram: an accurate representation of the distribution of numerical data that provides an estimate of the probability distribution of a continuous variable or to show frequency distributions

Isotopes: variants of a chemical element which differ in neutron number and consequently in nucleon number. All isotopes of a given element have the same number of protons (atomic number) but different numbers of neutrons (atomic mass) in each atom

Joseph's projection method: This method is used for 3D projections. In this method, the integral between two points is calculated to find the principal direction of the ray, first. Then, the other directions are obtained. Then, linear interpolation is done on the intersection points of the each of the planes (the ones not in the principal direction) in the sampling grid. The sum of these interpolations is used to compensate for the longer traversal of rays deviating from the principal direction.

Modules: distinct self-contained components or units of a system that are interrelated to other units to build a system. Each unit performs only one functionality and is combined to perform the complex activity of the system

OpenGL: It is a cross-language and cross-platform API used for rendering 2D and 3D vector graphics. It has a common set of commands that are used to control the graphics.

Point Spread Function (PSF): It describes the response of an imaging system to a point source or a point object like an impulse response. The degree of spreading (blurring) of the point object is a measure for the quality of an imaging system. It is used to enhance the resolution of the image during reconstruction.

Radiolabel: the technique of attaching or tagging a radioactive molecule to another molecule (such as a protein) so that it can be identified in the body. The radiolabeled substance emits positrons that can be picked up by a special scanner

Radioisotopes: unstable form of an element that emits radiation to transform into a more stable form

Run management: a record of the details of each run (a set of events) and the different configuration of the experiment set-up between runs

Sinogram: also referred as radon transform, is a visual representation (array of data containing the projections) of the raw data obtained in the operation of tomography that is used for image reconstruction

Tomography: the technique of using rotating X-rays or gamma rays to capture an image at a particular depth in the body, bringing those structures into sharp focus while blurring structures at other depths

Tracer: a substance (usually radioactively labeled) which is injected into a body to be followed to gain information about metabolic or biological processes

Tracking: a simulation of the passage of a particle through matter and considers the possible interactions and decay processes

User interface: an industrial design or visual representation of human–computer interaction; it is the space where interactions between humans and machines occur

Visualization: any technique for creating images, diagrams or animations which provides an effective way to communicate or represent a model

Chapter 1

INTRODUCTION

Positron Emission Tomography (PET) is a diagnostic tool used in the field of nuclear medicine for studying the functionality of a patient. PET has evolved in the last couple of decades and now plays a vital role in the health-care system as an indispensable tool for cancer diagnosis. The field of nuclear medicine always needs improvement and optimization of the system and examination protocols. Hence, understanding the scanner geometry and the underlying processes and how they affect the final result is of utmost importance. Since designing and testing on an actual system is very expensive and impractical, simulation and analysis of a realistic model of the system are becoming a fundamental process, providing a better visualization of the system and understanding of the system behavior.

GATE is a software, dedicated towards emission tomography that utilizes the Geant4 kernel, to model comprehensive scanner geometries and well-validated physics to simulate particle propagation. GATE is user-friendly and uses scripts for development. Its unique feature is its capacity to handle time-dependent processes that allows for coherent and realistic simulations. Monte Carlo method or simulation is a good tool to gain a better understanding of the whole system. It is a statistical tool that utilizes random numbers to solve complex problems. Using GATE with Monte Carlo model provides a tool for better improvement and optimization of the system.

The question of whether the simulated data can be trusted or not, can be answered with validation of the model by comparing its results with an actual system. This can be done by following the NEMA protocols for the model.

Therefore, the aim of this thesis was to gain an understanding of the PET systems, Monte Carlo method, modeling and simulation in GATE software, image reconstruction and analysis in CASToR software and testing their validity. This was done by simulating a realistic phantom with an activity distribution similar to that of a clinical exam using ^{18}F radioisotope in a modeled PET system using the GATE Monte Carlo software. Data acquired from the simulations and measurements were used to perform analysis and also, image reconstruction with CASToR.

Chapter 2

POSITRON EMISSION TOMOGRAPHY

2.1 Introduction

Positron Emission Tomography (PET) is a functional medical and nuclear imaging technique which utilizes the physical characteristics of radionuclides decayed by positron emission. It provides in-vivo molecular 3D imaging of the living processes inside the body relying on radioisotopes usage. It measures metabolic activity of the cells of body tissues as an aid to the diagnosis of disease. It is both a medical and research tool.

2.2 History

The beginning of PET history can be traced back to the postulation of the existence of positive electrons made by Dirac in 1930 ^[1]. Second, the production of suitable radioisotopes for medical applications and the first suitable gamma detector was made with the discovery of the inorganic scintillator NaI:Tl by Hofstadter in 1949 ^[1]. Third, the reconstruction of 3D images from the detected coincidence events based on the Radon transform first proposed in 1917 ^[1].

These lead to the development of the first PET prototype by Brownell and Sweet in 1953 ^[4] which consisted of a pair of opposed NaI:Tl crystals coupled to two photomultiplier tubes. These tubes acted in coincidence and mechanically moved in two dimensions to produce an image of the positron source through an embedded printing system.

The introduction of Bismuth Germanate (BGO) as replacement to NaI provided a dense and reasonably bright scintillator and dramatically improved the sensitivity of PET scanners. The introduction of the block detector geometry allowed to increase the spatial resolutions of the PET systems ^[1].

Though, there are alternative methods of scanning which includes x-ray computed tomography (CT), magnetic resonance imaging (MRI) and functional magnetic resonance imaging (fMRI), ultrasound and single-photon emission computed tomography (SPECT), the most important advancement that made PET an indispensable clinical device was the introduction of PET/CT scanners which was first proposed by Townsend and Nutt in 2000 ^[1].

2.3 Radiotracers used

The materials that are used for the radioactive nuclei as sources of emission of positrons in the PET systems are mainly ¹¹C, ¹³N, ¹⁵O, and ¹⁸F. These materials emit radiation and undergo radioactive decay. The most powerful radiation is γ (gamma) radiation. The gamma (γ) rays are a form of electromagnetic radiation with high energy photons like visible light or X-rays. However, they have a much shorter wavelength and a much higher energy. X-ray photons are generated by energetic electron processes whereas gamma ray photons are generated by nuclear decay.

The gamma ray spectrum is usually defined in the frequency between 10^{18} and 10^{21} Hertz. The radiation is the result of atoms losing some particle or particles (atomic degeneration process) called radioactive decay. These radioisotopes are incorporated in a

wide variety of radiopharmaceutical applications that are inhaled or injected which provide medical diagnosis based on images obtained from a PET system. The shorter the distance travelled by the emitted positrons, the more accurate the final image is generated. The energy of the photon is proportional to its frequency (ν), by a constant factor – Planck’s constant(h).

$$E = h \nu = h f \text{ (or) } f = E / h$$

Table 1. Positron-Emitting Radiotracers [2-3]

Radioisotope	Half-life	Production
Carbon-11	20.4 minutes	Cyclotron-produced
Fluorine-18	109.8 minutes	Cyclotron-produced
Nitrogen-13	10 minutes	Cyclotron-produced
Oxygen-15	2.03 minutes	Cyclotron-produced
Germanium-68	288 days	Generator-produced
Strontium-82	25 days	Generator-produced
Zinc-62	9.3 hours	Generator-produced
Copper-62	9.7 minutes	Generator-produced (daughter of Zinc-62)
Gallium-68	68 minutes	Generator-produced (daughter of Germanium-68)
Rubidium-82	1.25 minutes	Generator-produced (daughter of Strontium-82)
Yttrium-86	14.7 minutes	Generator-produced (daughter of Strontium-86)

Table 2. β^+ -emitters and their energy characteristics [3-4]

Radioisotope	Maximum positron energy (MeV)	Maximum positron range in water (mm)
Carbon-11	0.959	2.16
Fluorine-18	0.633	2.4
Nitrogen-13	1.197	4.88
Oxygen-15	1.738	7.92

2.4 Operation

PET systems are based on the detection of coincidence of the two 511 keV γ -rays emitted in opposite directions, produced by an electron-positron annihilation. These gamma rays follow the conservation of energy and momentum physics laws. The PET systems map the distribution of the positron emitting radio-tracer inside the body of a patient. This is done by injecting a specific molecule (radioisotope) marked with a β^+ -emitter, tracing a particular metabolic process into the patient. As the radioisotope undergoes positron emission decay (also known as positive beta decay), it emits a positron.

The emitted positron travels in tissue for a short distance during which time it loses kinetic energy, until it decelerates to a point and can interact with an electron in the tissue. The encounter annihilates both the electron and the positron, producing a pair of back-to-back 511 keV annihilation (gamma) photons moving in approximately opposite directions. These photons are detected when they reach a scintillator in the scanning device and create a burst of light which is detected by the use of several pairs of detectors like photomultiplier tubes or avalanche photodiodes. The technique depends on simultaneous or coincident detection of the pair of photons moving in approximately opposite directions. Photons that do not arrive in temporal pairs (within a timing-window of a few nanoseconds) are ignored. The spatial distribution of the radio-tracer is then obtained by means of tomographic reconstruction.

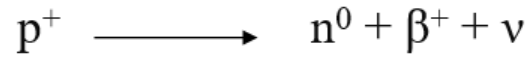


Figure 1. Positron decay – proton converted to a neutron, a positron and a neutrino [2]

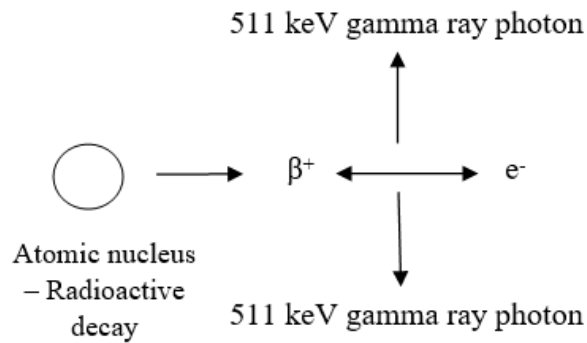


Figure 2. Positron annihilation reaction [2]

PET systems are capable of detecting areas of molecular biology detail (even prior to anatomic change) because of the usage of radiolabeled molecular probes with different rates of uptake depending on the type and function of tissue involved.

2.5 PET Scanner

The principle of a PET scanner is explained in figure 3 [5]. The patient is surrounded by an array of photodetectors and when a pair of gamma rays of the proper energy is detected within a coincidence time window, an event is assigned to the line connecting the two detectors. This line is called the Line of Response (LOR). In the recent applications, the preferred choice of detectors for PET application is by coupling a scintillating material to a photodetector.

As scintillators are dense crystalline structures which emit light (release energy) when an incident radiation interacts with it, they are used to convert one high energy photon into many low energy ones making it easier for detection by the photodetectors. The emitted light is in the visible or near ultra-violet range. This helps in preserving the information regarding the energy of the incident radiation. The number of photons produced is proportional to the energy deposited.

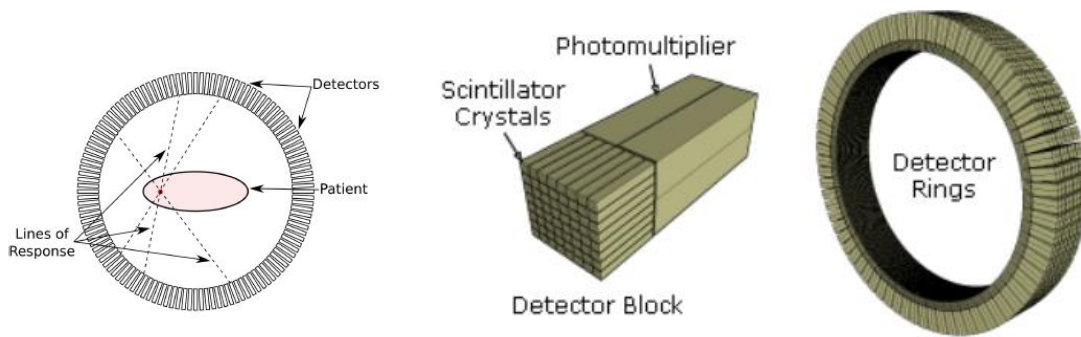


Figure 3. Schematic view of detector block with PMT example

Accumulating several LORs over acquisitions and processing the signals allows production of the 3D image of the tracer distribution in the patient. This is done by intersecting the Lines of Response (LORs) to reconstruct the original emitter position and by using image reconstruction algorithms. This allows measuring important body functions, such as blood flow, oxygen use, and glucose metabolism.

The most suitable scintillators for PET applications are BGO, LSO and LYSO ^[5] because of their density, light yield, decay constant and fast scintillation profile.

Table 3. Properties of common scintillators used in PET applications

	Density [g/cm ³]	Light Yield	Decay time [ns]	$\mu_{511\text{ keV}}$ [cm ⁻¹]	Emission [nm]
NaI:Tl	3.67	38000	230	0.34	415
BGO	7.13	9000	300	0.96	480
LSO:Ce	7.4	30000	40	0.87	420
LYSO:Ce	7.1	32000	40	0.82	420
LuAP:Ce	8.34	10000	17	0.95	365
LaBr ₃	5.08	61000	35	0.47	358

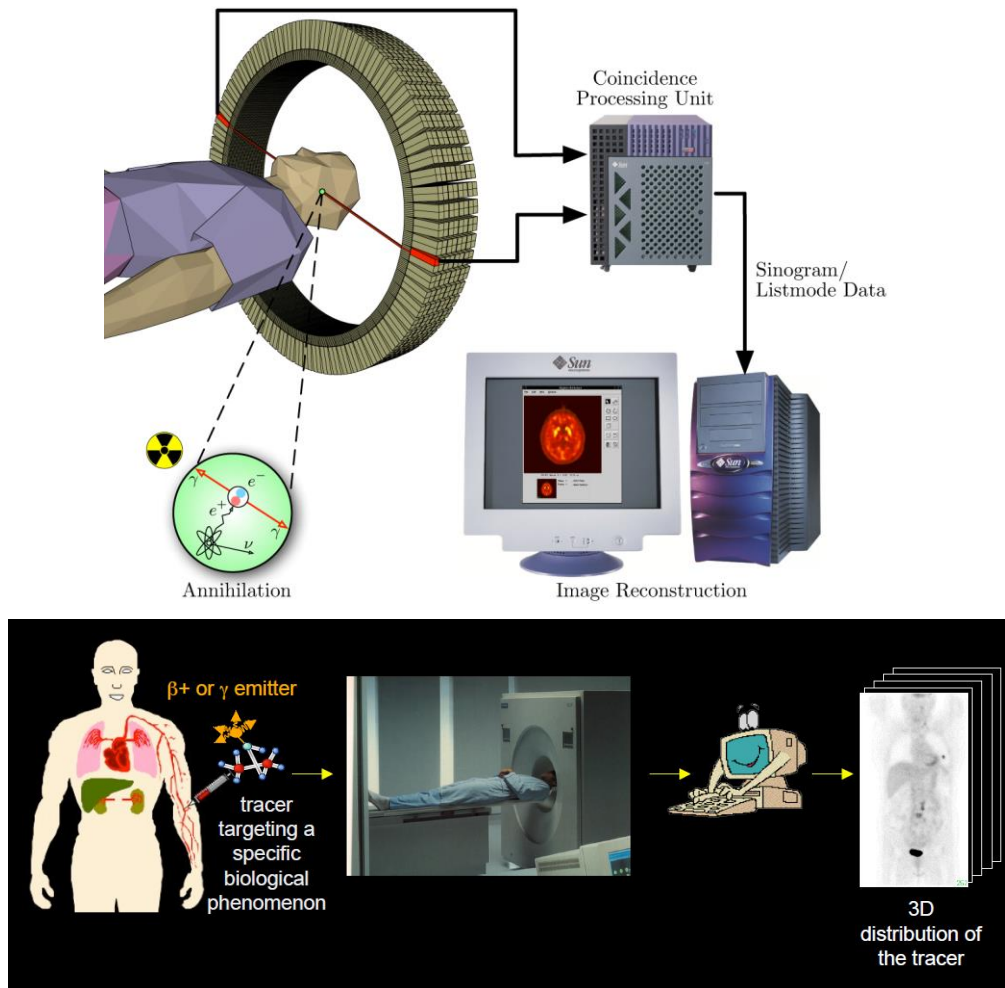


Figure 4. Schematic views of PET acquisition process

There are two approaches to reconstruct data from such a scanner. One is by treating each ring as a separate entity and detecting only coincidences within a ring. The image from each ring can then be reconstructed individually (2D reconstruction). The other method is to allow coincidences to be detected between rings as well as within rings. Then, reconstruct the entire volume together (3D reconstruction).

The 3D techniques have better sensitivity because more coincidences are detected and used. Hence, they have less noise but are more sensitive to the effects of scatter and random coincidences. The advent of sub-nanosecond timing resolution detectors provides better detection of true coincidence and random coincidence rejection.

2.6 Time-of-flight (TOF)

This is a new technique in PET systems with higher time resolution, used to improve the overall performance.

It measures the time difference between the detection of the pair of 511 KeV gamma rays (coincidence photons) precisely using the gamma-ray detectors and fast data processing systems. This helps in more accurate localization of the annihilation event along the line of response (LOR). The location accuracy is proportional to the system's time resolution. The location is given by the formula,

$$X = ((T2 - T1) * c) / 2, \text{ where } c = \text{speed of light}$$

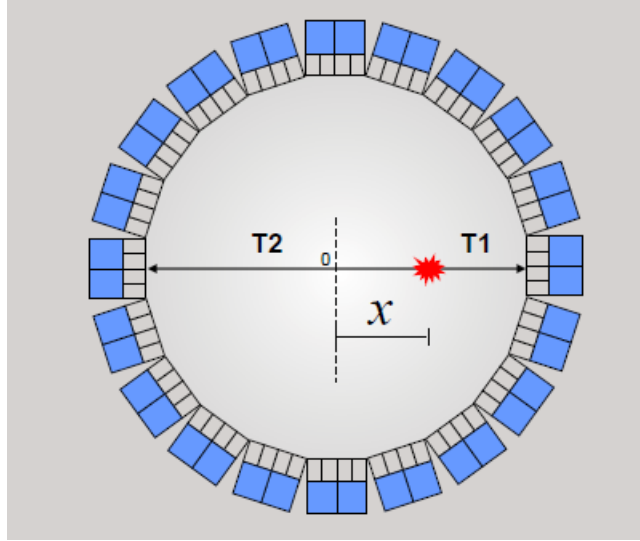


Figure 5. Event localization using ToF technique

It is histogrammed to quantify Coincidence Timing Resolution (CTR) ^[6]. This also provides a remarkable improvement in image quality, sensitivity amplification and noise reduction. It also improves the signal-to-noise ratio (i.e.) as the timing resolution improves, the SNR of the image will improve as well.

2.7 Depth of Interaction (DOI)

DOI information is provided by the vertical position of the source and the crystal and is obtained along the main axis of the scintillator ^[6-7]. This is the fundamental information required to reduce parallax error and achieve high performance for spatial resolution ^[5]. DOI resolution is independent of the position of the crystal in the scintillator array ^[6].

2.8 Medical applications

PET can measure blood flow, blood volume, oxygen usage, tissue pH (acidity), glucose (sugar) metabolism, and drug activity. It is very useful in detecting the activity of cancer because malignant cells grow at a faster rate and they metabolize more sugar. PET detects metabolism within body tissues and, hence, differs from other nuclear medicine examinations as they detect the amount of a radioactive substance collected in body tissue in a certain location to examine the tissue's function. The general applications are:

- To diagnose dementias (conditions that involve deterioration of mental function because of large decrease brain metabolism of both glucose and oxygen) such as Alzheimer's disease
- To diagnose neurological conditions such as Parkinson's disease (progressive disease of the nervous system in which one has a fine tremor, muscle weakness and a peculiar type of gait), Huntington's disease (hereditary disease of the nervous system which causes increasing dementia, bizarre involuntary movements and abnormal posture), Epilepsy (brain disorder involving recurrent seizures which can be detected by pinpointing the nonfunctioning area (metabolic changes) of the brain causing seizures in the brain and Stroke
- To locate the specific surgical site prior to surgical procedures of the brain and evaluate the brain after trauma to detect hematoma (blood clot), bleeding, and/or perfusion (blood and oxygen flow) of the brain tissue

- For neuroimaging as it is based on the assumption that areas of high radioactivity are associated with brain activity and localization of seizure in brain
- For diagnosis, staging, and monitoring treatment of cancers, early detection of recurrence of tumors
- To detect the spread of cancer to other parts of the body from original cancer site
- To evaluate the effectiveness of cancer treatment
- To evaluate the perfusion (blood flow) to the myocardium (heart muscle) for determining the effectiveness of a therapeutic procedure
- To identify lung lesions/masses and assist in the treatment of lung cancer

2.9 Safety Concerns

Though PET scanning is non-invasive, it involves exposure to radiation because the tracer is radioactive. This exposure is limited, however, because the radioactive chemicals have short half-lives (breakdown quickly and removed from the body through the kidneys). The risk of long-term exposure or cumulative radiation exposure needs to be considered. The elderly, women who are pregnant or nursing or people may have an allergic reaction to the tracer or the contrast agent should not undergo a PET scan.

2.10 Limitations

- High costs of cyclotrons needed to produce the short-lived radionuclides
- Need for specially adapted on-site chemical synthesis apparatus to produce the radiopharmaceuticals after radioisotope preparation

Chapter 3

BACKGROUND OF MODELING AND SIMULATION OF PET SYSTEMS

3.1 Introduction

Modeling and Simulation have become a significant and indispensable methods in the research and development of the PET/CT imaging technology. Different software has been used for the purpose of modeling and simulation of the PET system such as PETSIM, SimSET and Eidolon [7-8]. However, these softwares have some limitation in the flexibility of simulation of the system and the construction of the geometric characteristics construction of detectors. Widely used and tested general purpose nuclear physics codes packages such as Geant4 [8-9] have well-validated physics models and geometry modeling tools. However, adapting these codes to model various PET scanner geometries is difficult.

To overcome these limitations, GATE was developed. GATE is simulation software that uses Monte Carlo method and re-encapsulates the physical functionality of Geant4 software to make it a dedicated simulation software for nuclear medicine imaging [7][10]. After the system is modeled and simulation is done on GATE software, ROOT [11-12], STIR [13] and CASToR [14-15] can be used to process the acquired simulation data for data conversion and image reconstruction. Finally, the reconstructed image can be shown by ImageJ, AMIDE or other image viewer applications.

In the following, MC method (for data optimization and numerical integration) and the predecessors of GATE (SimSET, PETSIM, Eidolon and Geant) are discussed. Then, a detailed description of the GATE software is provided. Also, a brief description of the ROOT software for the analysis of the GATE output (from simulation), CASToR software and AMIDE tool for image reconstruction is given.

3.2 Monte Carlo simulation

Monte Carlo methods are numerical calculation methods based on the simulation using random variables. This technique has been applied to solve the mathematical problems since 1770 ^[16]. With the advent of quantum mechanics and matter radiation interactions interpreted using cross sections as probabilities, the random sampling technique (named Monte Carlo method) was applied to nuclear physics. In the early 1960s, H. O. Anger used this method to simulate the physical response of a new scintillation camera. Since then, Monte Carlo method has been extensively applied in medical radiation physics and Nuclear Medicine to solve a wide range of problems that could not be easily addressed by an experimental or analytical approach. Hence, Monte Carlo simulations are essential tools to assist in designing new imaging systems.

In Nuclear Medicine, particularly in SPECT and PET, the use of Monte Carlo methods was advantaged by the possibility of two types of Monte Carlo codes: 1) general purpose codes for simulation of particle transport developed for high energy physics or for dosimetry and 2) dedicated codes, designed specifically for SPECT or PET simulations (emission tomography configurations). Monte Carlo simulations of emission

tomography have proven to be useful to assist the detector design and to optimize acquisition and processing protocols. By creating a more realistic simulation, a straightforward extrapolation of conclusions comparable to the clinical environment are obtained. Therefore, such models can be used for system optimization, optimization of data acquisition protocols, improving data analysis and image quantification. These simulations are well suited for parallelization.

However, there are few concerns about a Monte Carlo simulation in nuclear medicine: its performance, versatility, validation and CPU-intensive simulations which often take up to several days to complete with state-of-the-art single-CPU computers.

3.3 SimSET

The Simulation System for Emission Tomography (SimSET) is an open source package that uses the Monte Carlo techniques to model the physical processes and instrumentation used in emission imaging. After its first release in 1993, SimSET has been a primary resource for many nuclear medicine imaging research groups around the world. The software is written in a modular format. The University of Washington Imaging Research Laboratory is continuing to develop SimSET, adding new functionality and utilities. The block diagram of the various modules that comprise SimSET is shown in Figure 6.

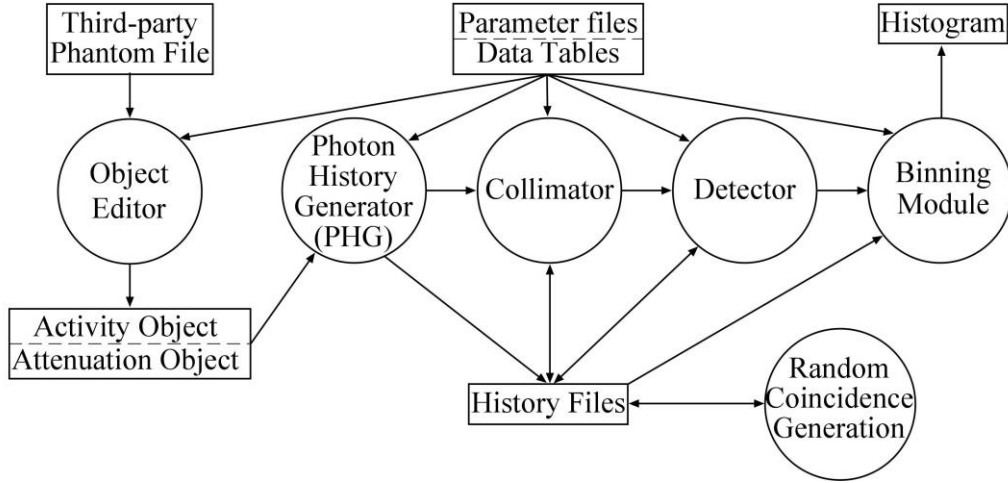


Figure 6. Block diagram of the various modules of SimSET

3.4 PETSIM

PETSIM is a dynamic PET simulator which takes an MRI image volume segmented into regions (each region corresponding to an activity) and generates a simulated PET volume. This software has been useful for the design of new PET scanners and for understanding the performance of commercial PET scanners. It was used extensively in the design of the PEM-I scanner for detecting breast cancer, and for the optimization of removable shielding, the NeuroShield, for use during brain scanning on a conventional whole-body PET scanner. It was used to estimate important parameters of the scanner and its performance before committing to a specific design.

3.5 EIDOLON

Eidolon is an open-source package written in Objective-C. It was developed initially as a part of the ParaPET project and is being continued to be funded by the Swiss National Foundation. It provides a framework for testing, reconstruction, attenuation and scatter correction methods for PET. It simulates a conventional multi-ring PET device and analyzes the generation of annihilation events using phantoms. It also allows the use of voxelized phantoms, complex shapes and geometries, provides the emission and attenuation distributions (known a priori).

3.6 Geant4

Geant4 (Geometry and Tracking) ^[17] is a software platform for the simulation of the transportation of particles through matter using Monte Carlo methods. It is well suited for the development of computational tools for analyzing interactions of particle with matter. Geant4 is the successor of the Geant series of software toolkits developed by CERN. It was the first toolkit to use object oriented programming (C++) for its development. It is maintained and supported by the international Geant4 Collaboration. It provides facilities for handling geometry, tracking, detector response, run management, visualization and user interface. It also performs basic histogramming. This helps in the reduction of time on low level details and provides basis for concentration on the more important aspects of the simulation.

It is widely used by a number of research projects around the world and applied in the areas of high energy physics (radiation effects in microelectronics where ionizing effects on semiconductor devices affect the device performance) and nuclear experiments, medical research (interactions of radiations used for treatment), accelerator and space physics (interactions between the natural space radiation environment and space hardware or astronauts) studies.

3.7 GATE (Geant4 Application for Tomographic Emission)

a) Introduction:

GATE ^[18-19] is an advanced open source Monte Carlo simulation software developed by the international OpenGATE collaboration. It is dedicated to perform numerical simulations in medical imaging and radiotherapy. It has the ability to realistically model nuclear medicine emission tomography. It encapsulates the well-proved Geant4 libraries to achieve a modular, versatile and object-oriented simulation platform for solutions. It is specifically adapted to the field of nuclear medicine and currently supports the following simulations:

- Emission Tomography (Positron Emission Tomography - PET and Single Photon Emission Computed Tomography - SPECT)
- Computed Tomography (CT)
- Optical Imaging (Bioluminescence and Fluorescence)
- Radiotherapy experiments

It plays a key role in the design of new medical imaging devices, optimization of acquisition protocols, development and assessment of image reconstruction algorithms and correction techniques. It allows describing time-dependent phenomena such as detector or patient movements, source decay kinetics and dead time for coincidence acquisitions including delay coincidences measurement. Thus, it allows the simulation of time curves under realistic acquisition conditions.

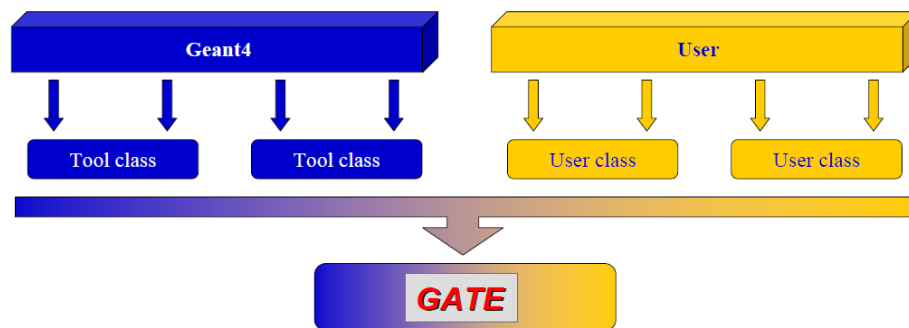


Figure 7. General structure of GATE

It includes all Geant4 well-validated features with the addition of a visualization tool and scripting (macro) language to command the simulations. With scripted language, users can specify the scanner geometry, movements of the scanner and phantom, radioisotope decays, etc. Single and/or coincidence detections of gamma rays by the crystals can be stored on an event-by-event basis into output files.

b) History:

The origin of GATE can be traced back to a workshop in Paris involving French and European labs in July 2001 ^[18]. It was a 2-day brainstorming meeting on Monte Carlo simulations and the decision was taken to develop a new code, based on Geant4, to

overcome the limitations of existing codes under the leadership of Christian Morel (EPFL, Lausanne).

The general consensus for the selection of Geant4 was to foster long-term support and maintenance by sharing the code development among many research groups. The first developments of the code started in December 2001, with 4 labs deeply involved at first (EPFL Lausanne, LPC Clermont Ferrand, University of Ghent, U494 Inserm Paris).

In early 2002, OpenGATE collaboration was established and more labs joined the collaboration for the development of the code. In May 2004, GATE was first released for public use. It is a project currently funded by French Research Agency, French Research Cancer Institute (Physicancer IMADRON) and European Commission (FP Cooperation: ENVISION project).

c) Features:

It is based on Geant4 (written in C++) and can be run on many platforms (Linux, Unix, MacOS, Windows (using virtual machine GATE version)). It is user-friendly (simulations can be designed and controlled using macros, without any knowledge in C++). It is flexible enough to model almost any detector design, including prototypes and provides explicit modeling of time. It can handle voxelized and analytical phantoms. Since it has modular design, new extensions can be easily added. It can run on a cluster architecture and on a grid. It supports modeling of time dependent processes and modeling the electronic response.

Modeling of the time-dependent processes supports change of tracer distribution over time, detector motions during acquisition, patient motion, moving phantoms, radioactive decay, dead times of the detector, time-of-flight, tracer kinetics. The principle of time modeling in GATE involves a customized Geant4 radioactive decay module, a clock to model the time changes during the experiment, experiment timing (time slices) defined by the user, time-dependent and synchronized objects update when time changes.

Modeling of the electronic response of the system involves linear signal processing, modular set-up via scripting, several dead time models to accurately reproduce count rate curves. It integrates Monte Carlo modeling tools with CT for implementing common coordinate system and, common object description, consistent sampling and convenient assessment of multimodality imaging.

It has a material database (can be edited/updated by user) by which any kind of materials can be defined by knowing its atomic numbers and percentage. It has the ability to simulate the conversion of photon interactions into digital counts in an attempt to model the detector and electronic responses of a real scanner.

d) Design and simulation:

The design of a GATE simulation is done using structural commands, each command performing a specific function. The commands can either be entered directly in the prompt after starting GATE (interactive) and be called upon using a macro file (ASCII-files with the extension .mac) for batched simulation. The macros are where a line contains a command to be executed, the order in which the commands are written will

determine the order in which the commands are interpreted by the prompt. Lines that start with a # will be seen as a comment. A macro file can call another macro file. GATE commands are organized as a tree structure. A complete simulation script should be defined in eight steps to be followed by the user as shown below:

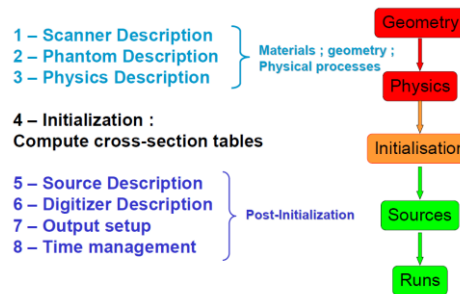


Figure 8. Steps for simulation

In step 1 (scanner description), the geometry for each volume that are components of the imaging device and the imaged object, are defined. These volumes are arranged in a volume hierarchy and each volume has a few specific properties such as size, position, and material composition. All the volumes are defined inside the world volume which is the top volume. The cylindricalPET system is based on a cylindrical geometry and it consists of 5 hierarchic levels: rsector, module, submodule, crystal and layer. When a volume needs to be repeated, such as crystals or block, repeater modules are defined.

For PET, cubic array or ring repeater is used. The materials for all these are obtained from the material database. To visualize the volumes, the graphics systems available in GATE are used in stored and immediate mode. The most common graphic system used is OpenGL. To save information regarding the hits occurring in the volumes of the crystal, crystal should be defined as sensitive.

In step 2 (Phantom description), the geometry of the volume to be scanned is defined within the world volume. To obtain information about the full gamma tracking from the vertex point to the end of gamma range in the experimental area with Compton, Rayleigh and photoelectric interactions, the phantom should be defined as sensitive. It will store two types of information – the number of scattering interactions generated in the phantom volume and the name of the physical volume in which the interaction occurred. This information is necessary in order to determine whether or not a photon reaching a detector has been scattered.

In step 3 (Physics description), the interaction processes for the simulation are defined. The models for physics processes are defined in the Geant4 library and they are incorporated as necessary for the model. The electromagnetic physics package manages the electrons, positrons, γ -rays, X-rays, optical photons, hadrons and ions. Two different packages can be used to simulate the electromagnetic processes: the standard energy package (photoelectric effect and Compton scatter can be simulated at energies above 10 keV) and the low energy package (treatment of photons and electrons down to 250 eV that includes Rayleigh scattering).

GATE provides the capability to set thresholds for the production of secondary electrons, X-rays and delta-rays to eliminate the secondary particles whose initial energy is below the production threshold. This helps in increasing the computing efficiency due to the increase in computing speed for the simulation.

In step 4 (Initialization), the initialization of the system is done. This triggers the calculation of the cross-section tables. The boundaries are checked as well. After this step, the geometry and the physics processes of the system cannot be modified.

In step 5 (Digitizer description), the electronics response of a detector within a scanner is simulated. The charged particle and photon interactions are converted into energy bins, the positions and coincidences are detected using the sensitive detectors. Sensitive detectors are used to store information about particle interactions (referred to as hits) within the physical volumes. Hits for those volumes that have a sensitive detector attached are the only ones that are stored. All information regarding interactions within non-sensitive volumes are discarded. The digitizer module consists of a chain of processing modules that takes each hit from the sensitive detectors and transforms them into pulses referred to as singles. At the end of a digitizer chain, a coincidence sort can be added to find the pairs of singles that are in coincidence. Pairs of singles can be considered as coincidences only when the time interval between the singles is less than the user-defined coincidence window. Each single is stored with its corresponding event number. If the event numbers of the singles associated in a coincidence are the same, then it is a true coincidence. If the event numbers of the singles associated in a coincidence are not the same, then it is a random coincidence. If the Compton scatter flag is used, then it is a scattered coincidence. (high energy electron can scatter the photons).

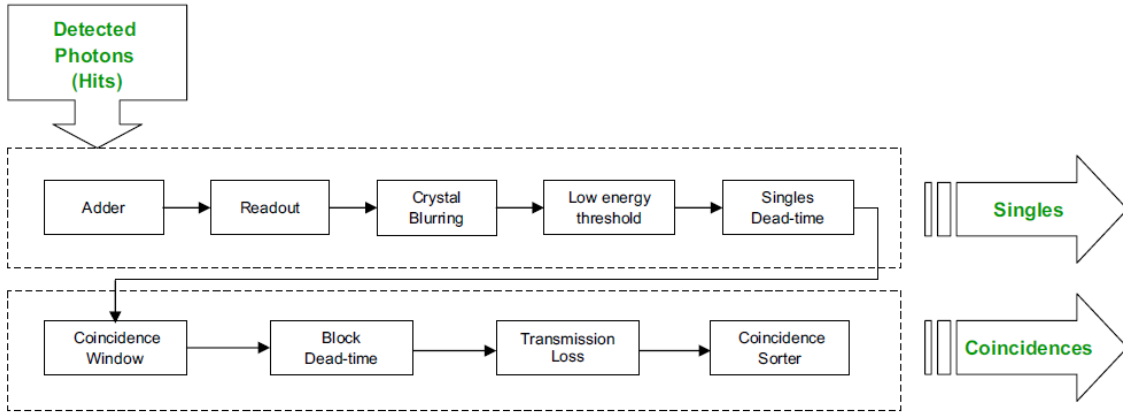


Figure 9. Flowchart for digitizer - Signal processing ^[20]

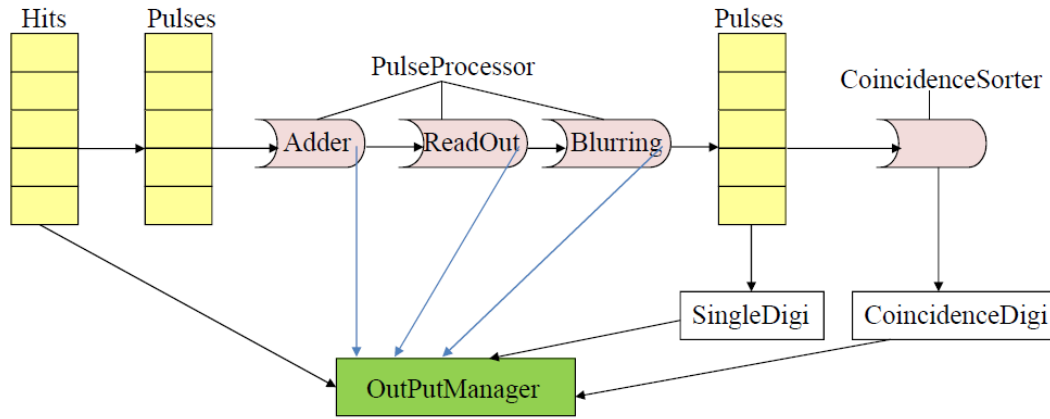


Figure 10. Block diagram for digitizer

GATE generates coincidences by opening a coincidence time window. When the first single event is detected, the model looks for other single events occurring within this window. This method constrains the second single event to not open its own. This model is referred to as the single window coincidence mode. In this mode, only one coincidence with events is generated. Another coincidence model is where each single event opens its own coincidence window and can thus be part of two different coincidences. This model is referred to as the multiple window coincidence mode ^[21]. In this mode, two

coincidences are generated. The random coincidences are intrinsically obtained by experimentally estimating the random coincidence rate by using a delayed coincidence window. Paralyzable or non-paralyzable dead times can be modeled on an event-by-event basis to avoid the loss of events during the coincidence time window.

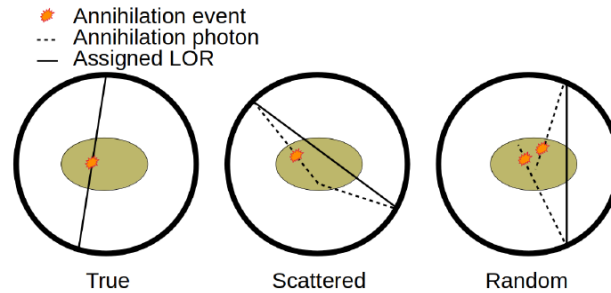


Figure 11. Depiction of the different coincidence events

In step 6 (Source description), a source (radioactive source represented by a volume in which the particles are emitted) is defined by its particle type (*e.g.* ion, gamma, positrons, etc.), position and geometry (volume), direction of emission (solid angle), energy (spectrum) and activity. The lifetime of unstable sources (radioactive ions) is usually obtained from the Geant4 database, but it can also be set by the user. The activity determines the decay rate of the source during the simulated acquisition time. The emission can also be confined to the intersection of the General Particle Source (GPS) and the confinement volume.

In step 7 (Output setup), the output data can be generated in several formats. These formats allow the user to analyze the simulation results at several levels. The common formats are ASCII (.dat extension) and ROOT (.root extension) output files

which can be transformed easily to a list mode file. For some scanner configurations, the events can be stored in a sinogram format or in List Mode Format (LMF). The output of the simulation software is a list of the single events, hits and coincidences detected.

Each line of the list gives the source ID, crystal ID, the energy, and the time stamp of each photon and data related to the list. The coincidence events consist of information of each detected annihilation photon pairs in terms of their origin information, energy, timing, the detector and crystal identification.

The time information taken into account for the generation of the output data are the time-steps that correspond to fixed positions of the scanner and the sources, decay times of the isotopes within the time-steps (including the Poisson nature of positron emission and the annihilation gamma's times of flight), dead-time applied on the singles and time window for coincidence acquisitions (which account for random, true and scatter coincidences, prompt and delayed coincidence count rates) ^[20].

In step 8 (Time management), the beginning and end of the acquisition process is defined along with the step time (time slice). Before the time, a random number generator engine and its seed are defined. At the beginning of each time-slice, the geometry is updated according to the user-defined movements. During each time-slice, the geometry is kept static and the simulation of particle transport and data acquisition occurs. Each slice corresponds to a run or projection.

3.8 ROOT

ROOT is a modular scientific software toolkit and a framework developed at CERN for data processing and analysis at the heart of the research on high-energy physics ^[12]. It is a powerful tool and provides all the functionalities required to deal with big data processing, statistical analysis, visualization and data storage. The ROOT files are self-descriptive.

ROOT allows the user to save data and any C++ object in a compressed binary form (including both the data and the description). ROOT provides a data structure, the tree, which is extremely powerful for fast access of huge amounts of data - orders of magnitude faster than accessing a normal file. Data saved into ROOT files can be accessed from PC, the web and large-scale file delivery systems such as GRID. If the ROOT trees are spread over several files, they can be chained and accessed as a unique object, allowing for loops over huge amounts of data.

3.9 CASToR

CASToR (Customizable and Advanced Software for Tomographic Reconstruction) is an open-source software platform developed for tomographic image reconstruction. It utilizes iterative reconstruction algorithms to reconstruct SPECT and PET data ^[18].

It utilizes a scanner geometry file (an ASCII file with characteristics unique to the scanner) to identify and give each detector element an identification number. This

identification number is used to identify all events that have occurred in the specific detector. A datafile is defined as a collection of events and is linked to a scanner geometry defined by the user.

It supports geometries of the PET, SPECT and CT system. The code is segmented into several main components including datafiles management, image processing, optimization algorithms, projectors, etc. It provides a utility tool to convert GATE Monte Carlo simulated data in ROOT format into the CASToR datafile format. It has commands for the estimation of corrections (scatter, random, true) for the given input data and provides full support for GATE datasets (data output, corrections). The important features of CASToR are listed below:

- Generic programming (abstract code)
- Flexibility and modularity
- Programming performed in standard C++
- No use of any external libraries as much as possible
- Iterative reconstruction algorithms
- Reconstruction of TOF PET list-mode and histogrammed data
- Optimization algorithm such as MLEM, One-Step-Late, MLTR, etc.
- Plug-in class systems for image convolution and general image processing
- Interfile I/O format for images

3.10 AMIDE (Amide's a Medical Image Data Examiner)

AMIDE ^[22] is an open-source and user-friendly tool for viewing, analyzing and rendering the medical imaging data sets. It is based on GTK+ toolkit for user interface and can run on any OS (Linux, Windows, Mac, etc.) which enhances its portability. It can display multiple data sets simultaneously which helps in easy comparison of the different systems or data sets. The tree-view of the study data provides a better understanding of the study and clear view during comparison between multiple data sets.

The display sets can be rotated, shifted, re-sized and magnified for analysis. It supports input from many medical imaging modeling softwares and various output data sets – file formats (raw data, interfiles, DICOM, etc.,) which makes it a versatile and important tool to view the reconstructed images from the simulations of the medical imaging devices, even for casual research users.

It also supports interpolation of the data sets and view based on Region of Interests (ROI). The studies are stored in XML-based directory format and they can be exported as any basic image formats (such as .jpg, .png) for further usage.

Chapter 4

MODELING AND SIMULATION OF PET SYSTEMS

GATE (version 8.0) is being used to build a model of PET using cylindrical PET template from GATE systems, to simulate particle propagation and to analyze the propagation. For the modeling of a PET system in GATE, the Ultra-High Resolution (UHR) PET system, High-resolution research tomography (HRRT) dedicated brain PET scanner system and the Biograph Vision whole-body clinical PET scanner system are being used as template. The main specifications and design characteristics ^[23] of these systems required for the modeling are as given in Table 4.

The HRRT and Biograph Vision systems are based on block detection technology. The advantage of this technology is that it reduces the cost and density of the sensors and the detectors (electronic channels). The disadvantage of this technology is that it leads to lower spatial resolution, image integrity and counting rate performance. To overcome these disadvantages, the UHR system is based on the LabPET II technology. This technology is based on 1:1 coupling of the scintillators and detectors (true pixelated detectors), thus, providing a high spatial resolution, high image quality, high precision and high reliability.

The 8-step method is followed to complete the model: scanner description, phantom description, physics description, initialization, source description, digitizer description, output setup, time management ^[24].

The specifications / dimensions for modeling each of the system are given in Table 4.

Table 4. Design specifications of UHR, HRRT and Biograph Vision PET scanners ^[23]

Parameters	UHR	HRRT	Biograph Vision
Scintillator material	LYSO	LSO/LYSO	LSO
No. of scintillators	129024	119808	60800
Scintillator size (mm ³)	1.12x1.12x12	2.1x2.1x(10+10)	3.2x3.2x20
Scintillator array dimension	4x8	72x104 (x2 layers)	10x20
Photodetector	APD	PMT	SiPM
Scintillator-to-Photodetector ratio	1:1	7488:140	200:128
Axial length (mm)	235	252	263
Ring radius (mm)	390	469	410
Transaxial FOV (mm)	271	312	700
Coincidence time window (ns)	6	6	4.73
Energy window (keV)	250-650	350-650	435-650
Dead time (ns)	490	320	320

4.1 World volume

All the systems modeled in GATE are defined inside the “world” volume. This volume is the base of the tree structure of the GATE systems. It is a box centered at the origin and encloses the geometry of the complete system within it. The simulation of the system (i.e.) the tracking of the particle is stopped at the boundary of this volume. The world volume is set to dimensions 1 x 1 x 1 m³ for all the three models. The different materials required for the volumes’ definition are obtained from the database file (GateMaterials.db).

```
#      W O R L D
/gate/world/geometry/setXLength      1.0 m
/gate/world/geometry/setYLength      1.0 m
/gate/world/geometry/setZLength      1.0 m
```

Figure 12 a. Code for world volume

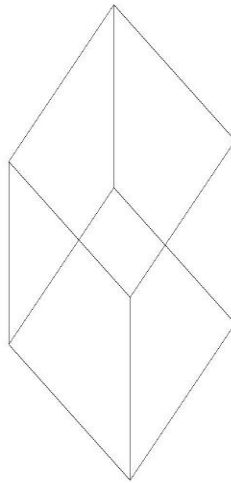


Figure 12 b. Simulated world volume

4.2 PET system selection

The cylindricalPET system is used and it is defined as the daughter volume of the world. The defined material is air.

The cylinder for the UHR has maximum radius of 390 mm, minimum radius of 152 mm and height of 235 mm (corresponding to axial FOV). It is centered from the origin of the mother volume (world).

```
# CYLINDRICAL
/gate/world/daughters/name cylindricalPET
/gate/world/daughters/insert cylinder
/gate/cylindricalPET/setMaterial Air
/gate/cylindricalPET/placement/setTranslation 0.0 0.0 0.0 mm
/gate/cylindricalPET/geometry/setRmax 390.0 mm
/gate/cylindricalPET/geometry/setRmin 152.0 mm
/gate/cylindricalPET/geometry/setHeight 235.0 mm
/gate/cylindricalPET/vis/forceWireframe
/gate/cylindricalPET/vis/setColor white
```

Figure 13 a. Code for cylindrical PET volume for UHR

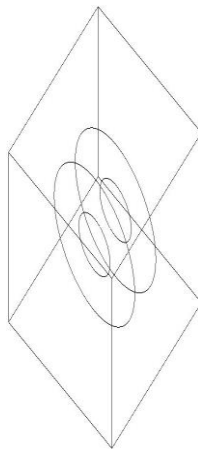


Figure 13 b. Simulated cylindrical PET volume for UHR

The cylinder for the HRRT has maximum radius of 469 mm, minimum radius of 155 mm and height of 252 mm (corresponding to axial FOV). It is centered from the origin of the mother volume (world).

```
# CYLINDRICAL
/gate/world/daughters/name          cylindricalPET
/gate/world/daughters/insert        cylinder
/gate/cylindricalPET/setMaterial    Air
/gate/cylindricalPET/placement/setTranslation 0.0 0.0 0.0 mm
/gate/cylindricalPET/geometry/setRmax 469.0 mm
/gate/cylindricalPET/geometry/setRmin 155.0 mm
/gate/cylindricalPET/geometry/setHeight 252.0 mm
/gate/cylindricalPET/vis/forceWireframe
/gate/cylindricalPET/vis/setColor   white
```

Figure 13 c. Code for cylindrical PET volume for HRRT

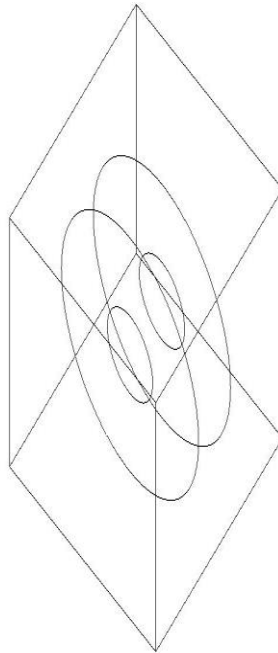


Figure 13 d. Simulated cylindrical PET volume for HRRT

The cylinder for the Biograph Vision has maximum radius of 410 mm, minimum radius of 290 mm and height of 263 mm (corresponding to axial FOV). It is centered from the origin of the mother volume (world).

```
# CYLINDRICAL
/gate/world/daughters/name          cylindricalPET
/gate/world/daughters/insert        cylinder
/gate/cylindricalPET/setMaterial    Air
/gate/cylindricalPET/placement/setTranslation 0.0 0.0 0.0 mm
/gate/cylindricalPET/geometry/setRmax 410.0 mm
/gate/cylindricalPET/geometry/setRmin 290.0 mm
/gate/cylindricalPET/geometry/setHeight 263.0 mm
/gate/cylindricalPET/vis/forceWireframe
/gate/cylindricalPET/vis/setColor   white
```

Figure 13 e. Code for cylindrical PET volume for Biograph Vision

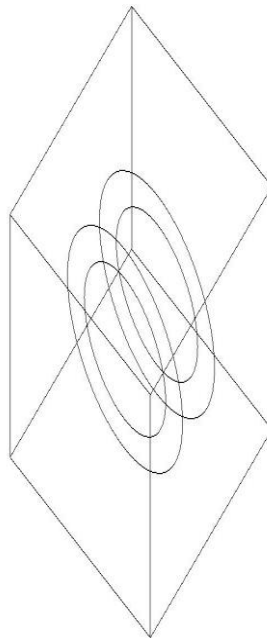


Figure 13 f. Simulated cylindrical PET volume for Biograph Vision

4.3 Defining scanner geometry

The cylindrical PET scanner system has 5 hierarchical levels to be defined. Each of these levels are defined as separate volumes as below:

- First volume is the rsector volume - Material is air
- Second volume is the block volume - an optional block. Here, it is not modeled in the HRRT system - Material is air
- Third volume is the sub-module - an optional block. It is not defined in all the three PET system models - Material is air
- Fourth volume is the crystal volume - Material is air
- Fifth volume is the layer volume – Material is the scintillating crystal for the three PET systems (LYSO or LSO)

The dimensions (specifications) for the layer level and the crystal level are based on the specifications given in Table 4. The dimensions of the other layers are based on the arrangement of the crystals on the y-axis and z-axis.

```
# RSECTOR
/gate/cylindricalPET/daughters/name          rsector
/gate/cylindricalPET/daughters/insert       box
/gate/rsector/setMaterial                    Air
/gate/rsector/placement/setTranslation       271.0 0.0 0.0 mm
/gate/rsector/geometry/setXLength           1.5 mm
/gate/rsector/geometry/setYLength           63.0 mm
/gate/rsector/geometry/setZLength           235.0 mm
/gate/rsector/vis/setVisible                 0
```

Figure 14 a. Code for rsector level / volume for UHR

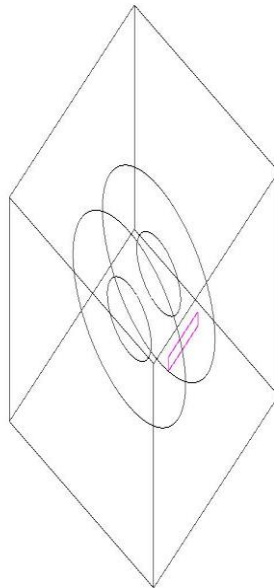


Figure 14 b. Simulated rsector level / volume for UHR

```
# RSECTOR
/gate/cylindricalPET/daughters/name      rsector
/gate/cylindricalPET/daughters/insert   box
/gate/rsector/setMaterial                 Air
/gate/rsector/placement/setTranslation   312.0 0.0 0.0 mm
/gate/rsector/geometry/setXLength        20.0 mm
/gate/rsector/geometry/setYLength        152.0 mm
/gate/rsector/geometry/setZLength        220.0 mm
/gate/rsector/vis/setVisible              0
```

Figure 14 c. Code for rsector level / volume for HRRT

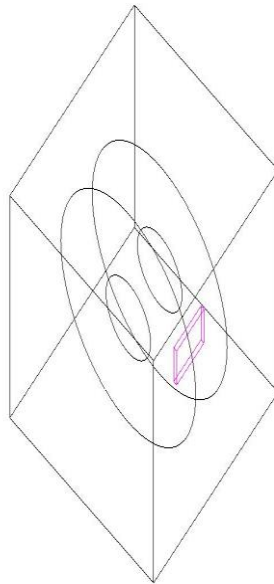


Figure 14 d. Simulated rsector level / volume for HRRT

```
# RSECTOR
/gate/cylindricalPET/daughters/name          rsector
/gate/cylindricalPET/daughters/insert       box
/gate/rsector/setMaterial                    Air
/gate/rsector/placement/setTranslation       350.0 0.0 0.0 mm
/gate/rsector/geometry/setXLength           20.0 mm
/gate/rsector/geometry/setYLength           64.0 mm
/gate/rsector/geometry/setZLength           256.0 mm
/gate/rsector/vis/setVisible                 0
```

Figure 14 e. Code for rsector level / volume for Biograph Vision

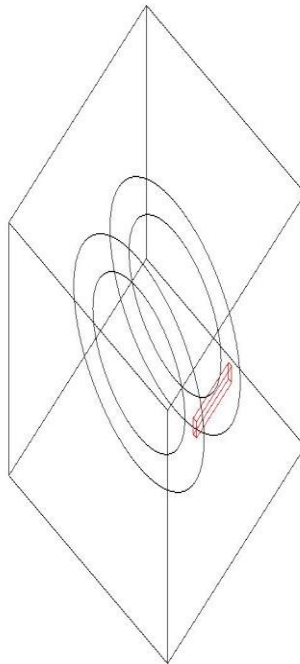


Figure 14 f. Simulated rsector level / volume for Biograph Vision

```
# BLOCK
/gate/rsector/daughters/name      block
/gate/rsector/daughters/insert   box
/gate/block/setMaterial          Air
/gate/block/placement/setTranslation 0.0 0.0 0.0 mm
/gate/block/geometry/setXLength  1.5 mm
/gate/block/geometry/setYLength  8.96 mm
/gate/block/geometry/setZLength  48.0 mm
/gate/block/vis/setColor         yellow
/gate/block/vis/setVisible       0
```

Figure 15 a. Code for block level / volume for UHR

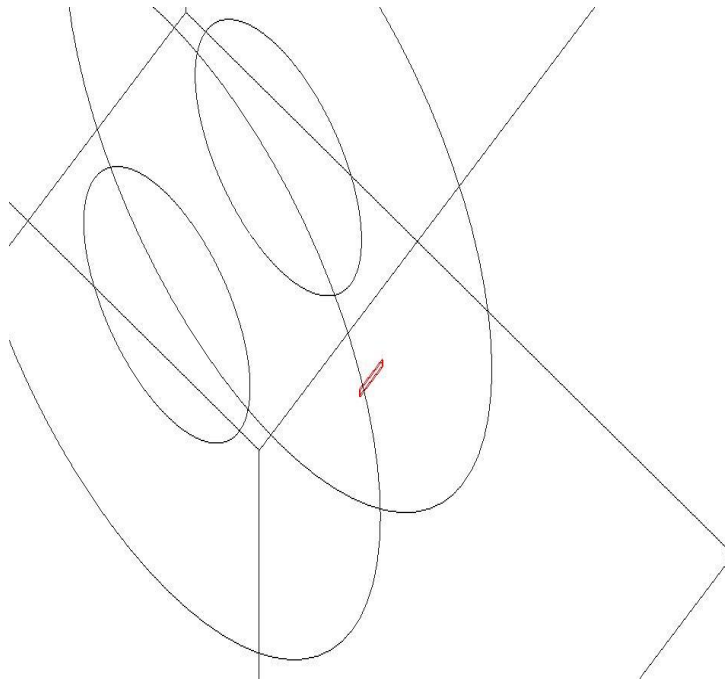


Figure 15 b. Simulated block level / volume for UHR

```
# BLOCK
/gate/rsector/daughters/name          block
/gate/rsector/daughters/insert       box
/gate/block/setMaterial               Air
/gate/block/placement/setTranslation  0.0 0.0 0.0 mm
/gate/block/geometry/setXLength       20.0 mm
/gate/block/geometry/setYLength       64.0 mm
/gate/block/geometry/setZLength       32.0 mm
/gate/block/vis/setColor              yellow
/gate/block/vis/setVisible            0
```

Figure 15 c. Code for block level / volume for Biograph Vision

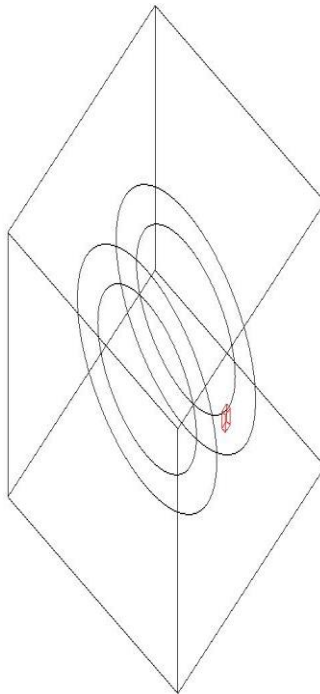


Figure 15 d. Simulated block level / volume for Biograph Vision

```
# C R Y S T A L
/gate/block/daughters/name          crystal
/gate/block/daughters/insert       box
/gate/crystal/setMaterial           Air
/gate/crystal/placement/setTranslation 0.0 0.0 0.0 mm
/gate/crystal/geometry/setXLength   1.12 mm
/gate/crystal/geometry/setYLength   1.12 mm
/gate/crystal/geometry/setZLength   12.0 mm
/gate/crystal/vis/setColor          blue
/gate/crystal/vis/setVisible        0
```

Figure 16 a. Code for crystal level / volume for UHR

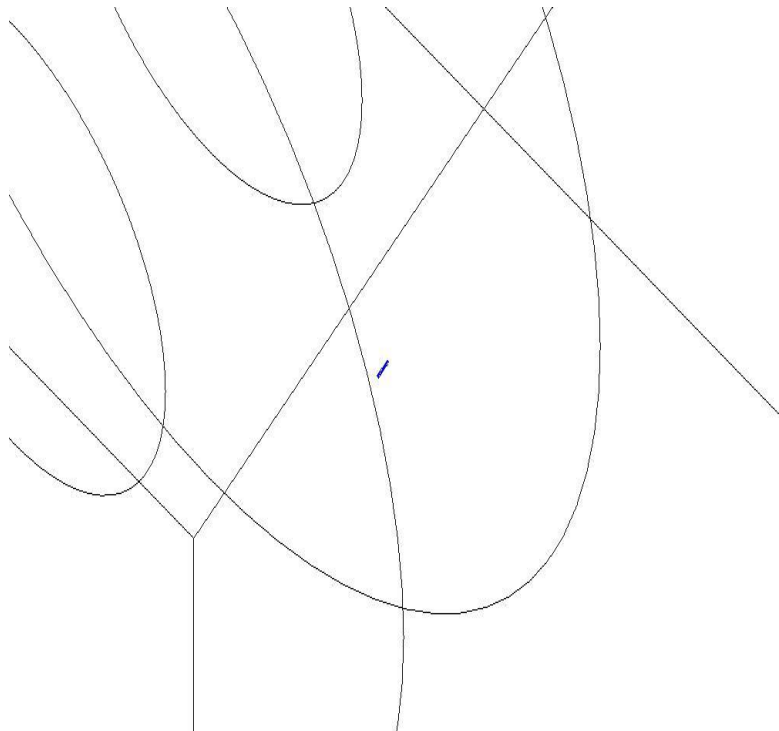


Figure 16 b. Simulated crystal level / volume for UHR


```
# C R Y S T A L
/gate/rsector/daughters/name          crystal
/gate/rsector/daughters/insert       box
/gate/crystal/setMaterial             Air
/gate/crystal/placement/setTranslation 0.0 0.0 0.0 mm
/gate/crystal/geometry/setXLength    20.0 mm
/gate/crystal/geometry/setYLength    2.1 mm
/gate/crystal/geometry/setZLength    2.1 mm
/gate/crystal/vis/setColor           blue
/gate/crystal/vis/setVisible         0
```

Figure 16 c. Code for crystal level / volume for HRRT

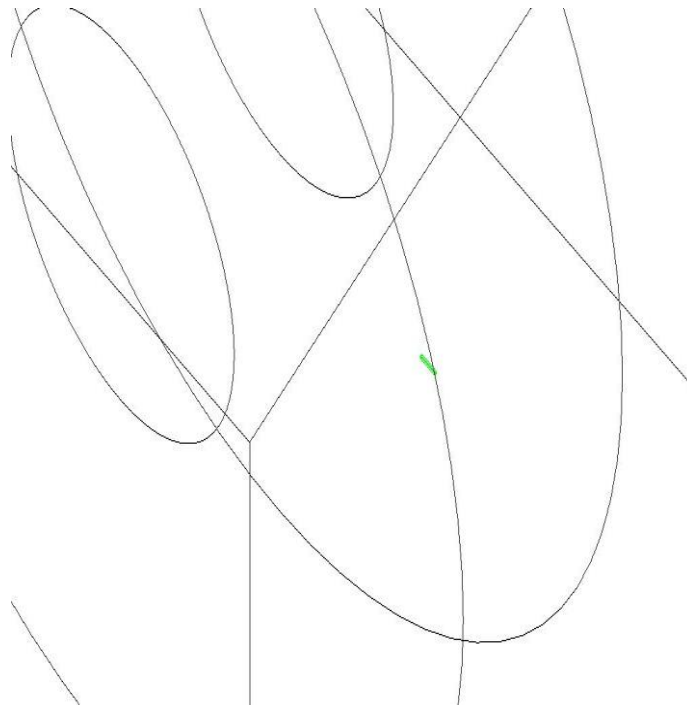


Figure 16 d. Simulated crystal level / volume for HRRT

```
# C R Y S T A L
/gate/block/daughters/name          crystal
/gate/block/daughters/insert        box
/gate/crystal/setMaterial            Air
/gate/crystal/placement/setTranslation 0.0 0.0 0.0 mm
/gate/crystal/geometry/setXLength    20.0 mm
/gate/crystal/geometry/setYLength    3.2 mm
/gate/crystal/geometry/setZLength    3.2 mm
/gate/crystal/vis/setColor           blue
/gate/crystal/vis/setVisible         0
```

Figure 16 e. Code for crystal level / volume for Biograph Vision

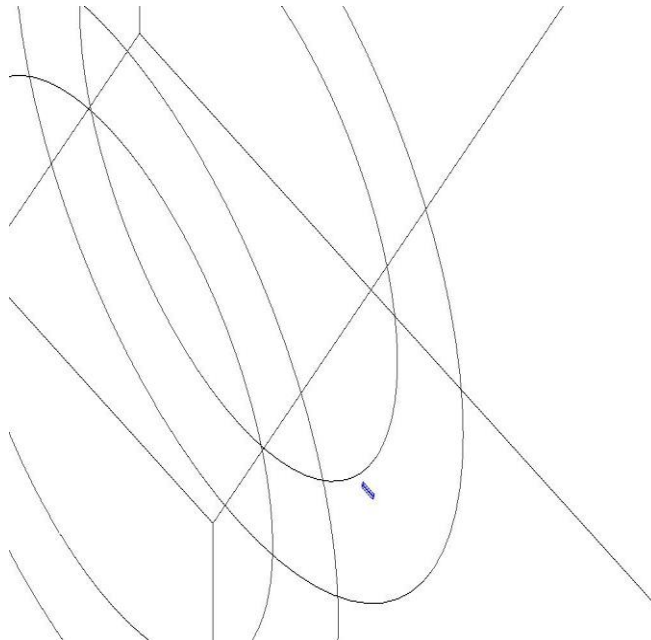


Figure 16 f. Simulated crystal level / volume for Biograph Vision

```
# LYSO layer
/gate/crystal/daughters/name      LYSO
/gate/crystal/daughters/insert    box
/gate/LYSO/setMaterial            LYSO
/gate/LYSO/placement/setTranslation 0.0 0.0 0.0 mm
/gate/LYSO/geometry/setXLength    1.12 mm
/gate/LYSO/geometry/setYLength    1.12 mm
/gate/LYSO/geometry/setZLength    12.0 mm
/gate/LYSO/vis/setColor           red
```

Figure 17 a. Code for layer level / volume for UHR

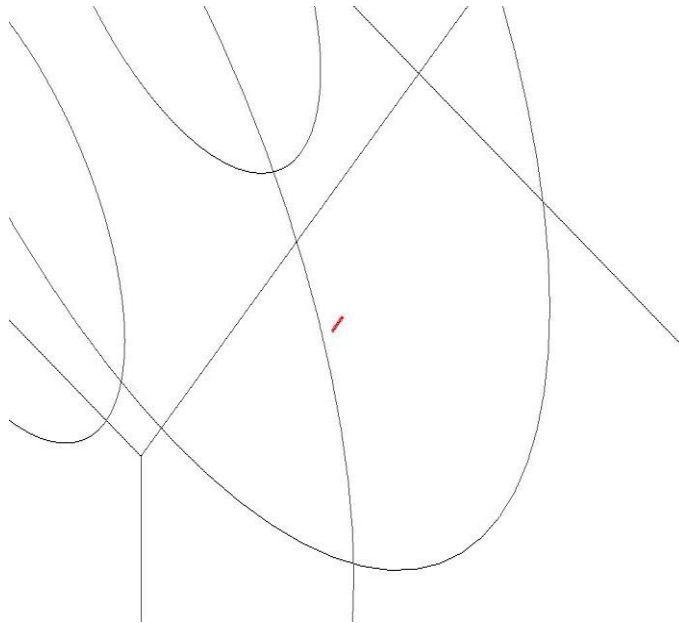


Figure 17 b. Simulated layer level / volume for UHR

```

# LSO layer
/gate/crystal/daughters/name          LSO
/gate/crystal/daughters/insert        box
/gate/LSO/setMaterial                  LSO
/gate/LSO/placement/setTranslation     -5.0 0.0 0.0 mm
/gate/LSO/geometry/setXLength          10.0 mm
/gate/LSO/geometry/setYLength          2.1 mm
/gate/LSO/geometry/setZLength          2.1 mm
/gate/LSO/vis/setColor                 yellow

# LYSO layer
/gate/crystal/daughters/name          LYSO
/gate/crystal/daughters/insert        box
/gate/LYSO/setMaterial                 LYSO
/gate/LYSO/placement/setTranslation     +5.0 0.0 0.0 mm
/gate/LYSO/geometry/setXLength          10.0 mm
/gate/LYSO/geometry/setYLength          2.1 mm
/gate/LYSO/geometry/setZLength          2.1 mm
/gate/LYSO/vis/setColor                 red

```

Figure 17 c. Code for layer level / volume for HRRT

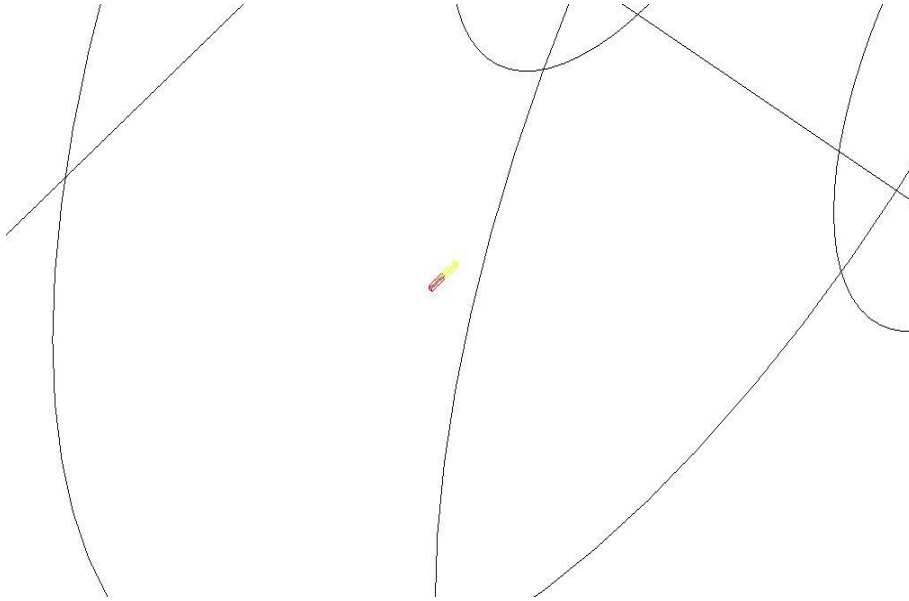


Figure 17 d. Simulated layer level / volume for HRRT

```

# LSO layer
/gate/crystal/daughters/name LSO
/gate/crystal/daughters/insert box
/gate/LSO/setMaterial LSO
/gate/LSO/placement/setTranslation 0.0 0.0 0.0 mm
/gate/LSO/geometry/setXLength 20.0 mm
/gate/LSO/geometry/setYLength 3.2 mm
/gate/LSO/geometry/setZLength 3.2 mm
/gate/LSO/vis/setColor red

```

Figure 17 e. Code for layer level / volume for Biograph Vision

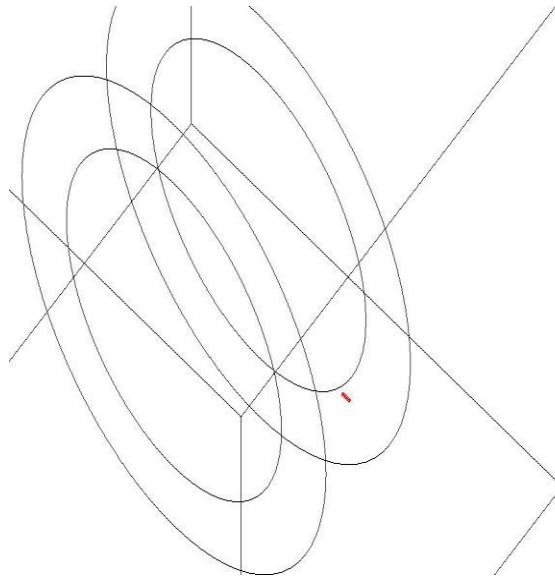


Figure 17 f. Simulated layer level / volume for Biograph Vision

After the levels are defined, the matrix of the crystals is defined. This is done by defining the repeater modules for the obtaining the complete ring detector. For this, three levels - the crystal level, the block level (not for HRRT) and the rsector level are repeated along any of the three directions.

The crystal level and the block level are along y-axis and z-axis to satisfy the number of scintillators per ring in Table 4. As the repetition is linear, cubicArray repeater is used for these two levels. The rsector level is repeated in a ring pattern to cover the complete radius of the cylindrical PET ring. Hence, ring repeater is used. This generates the total number of scintillators as per Table 4 for each of the scanner systems.

```
# REPEAT CRYSTAL
/gate/crystal/repeaters/insert cubicArray
/gate/crystal/cubicArray/setRepeatNumberX 1
/gate/crystal/cubicArray/setRepeatNumberY 8
/gate/crystal/cubicArray/setRepeatNumberZ 4
/gate/crystal/cubicArray/setRepeatVector 0.0 1.12 12.0 mm
```

Figure 18 a. Code for crystal level repeater for UHR

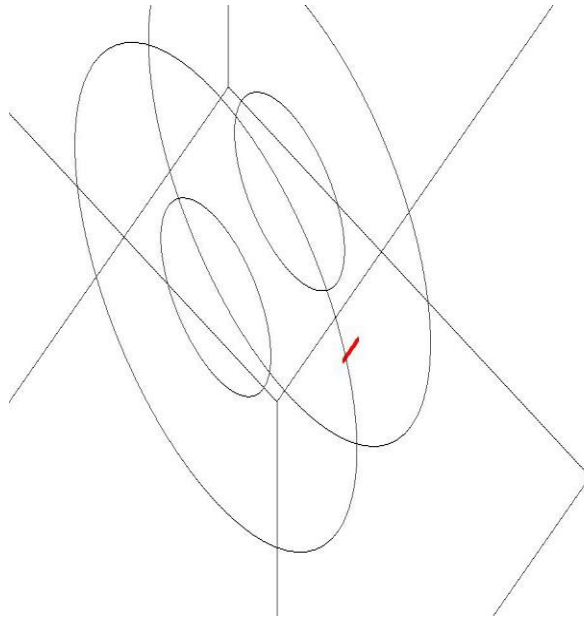


Figure 18 b. Simulated crystal level repeater for UHR

```

# R E P E A T   C R Y S T A L
/gate/crystal/repeaters/insert          cubicArray
/gate/crystal/cubicArray/setRepeatNumberX 1
/gate/crystal/cubicArray/setRepeatNumberY 72
/gate/crystal/cubicArray/setRepeatNumberZ 104
/gate/crystal/cubicArray/setRepeatVector 0.0 2.1 2.1 mm

```

Figure 18 c. Code for crystal level repeater for HRRT

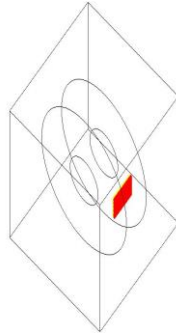


Figure 18 d. Simulated crystal level repeater for HRRT

```

# R E P E A T   C R Y S T A L
/gate/crystal/repeaters/insert          cubicArray
/gate/crystal/cubicArray/setRepeatNumberX 1
/gate/crystal/cubicArray/setRepeatNumberY 20
/gate/crystal/cubicArray/setRepeatNumberZ 10
/gate/crystal/cubicArray/setRepeatVector 0.0 3.2 3.2 mm

```

Figure 18 e. Code for crystal level repeater for Biograph Vision

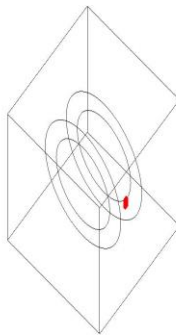


Figure 18 f. Simulated crystal level repeater for Biograph Vision

```

# R E P E A T   B L O C K
/gate/block/repeaters/insert          cubicArray
/gate/block/cubicArray/setRepeatNumberX 1
/gate/block/cubicArray/setRepeatNumberY 7
/gate/block/cubicArray/setRepeatNumberZ 4
/gate/block/cubicArray/setRepeatVector 0.0 8.96 48.0 mm

```

Figure 19 a. Code for block level repeater for UHR

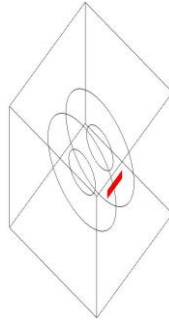


Figure 19 b. Simulated block level repeater for UHR

```

# R E P E A T   B L O C K
/gate/block/repeaters/insert          cubicArray
/gate/block/cubicArray/setRepeatNumberX 1
/gate/block/cubicArray/setRepeatNumberY 1
/gate/block/cubicArray/setRepeatNumberZ 8
/gate/block/cubicArray/setRepeatVector 0.0 0.0 32.0 mm

```

Figure 19 c. Code for block level repeater for Biograph Vision

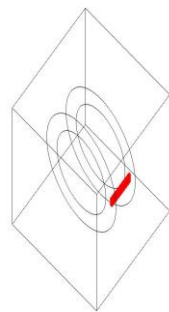


Figure 19 d. Simulated block level repeater for Biograph Vision


```
# R E P E A T RSECTOR
/gate/rsector/repeaters/insert          ring
/gate/rsector/ring/setRepeatNumber     144
```

Figure 20 a. Code for rsector level repeater for UHR



Figure 20 b. Simulated rsector level repeater for UHR

```
# R E P E A T RSECTOR
/gate/rsector/repeaters/insert          ring
/gate/rsector/ring/setRepeatNumber     8
```

Figure 20 c. Code for rsector level repeater for HRRT

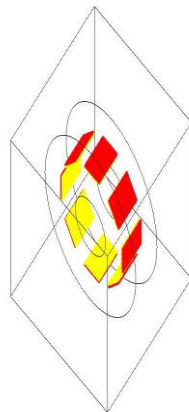


Figure 20 d. Simulated rsector level repeater for HRRT

```
# R E P E A T RSECTOR
/gate/rsector/repeaters/insert          ring
/gate/rsector/ring/setRepeatNumber     38
```

Figure 20 e. Code for rsector level repeater for Biograph Vision

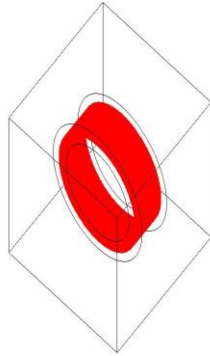


Figure 20 f. Simulated rsector level repeater for Biograph Vision

After the repeaters are defined, the scanner is connected to the system. To store information on the particle interactions (hits) within the detector volumes, they are defined as sensitive. GATE stores the hits information only for the volumes attached to a sensitive detector in an output format specified in the model. The information stored are energy deposition, position of interaction, origin of particle, momentum of particle, type of interaction, etc.

4.4 Defining phantom geometry

The phantom is the volume in which the scan occurs. Different phantoms are used for the analysis. The first phantom used is a NEMA NU4 standards phantom – a plastic cube of 10 mm on each side. This phantom is used for sensitivity and spatial resolution

assessment. The second phantom used is NEMA NU2 standards cylindrical phantom of 700 mm length and 200 mm diameter. This phantom is used for the count rate performance assessment.

Three different phantoms are used for image quality performance assessment. The first phantom used is NEMA 2 (NEMA IEC) standards. It has a body phantom, a lung insert and an insert with 6 spheres with different radius (10 mm, 13 mm, 17 mm, 22 mm, 28 mm and 37 mm). The second phantom used is NEMA 4 (NEMA IQ) standards with maximum radius as 15 mm, minimum radius (set by default) as 0 mm and height as 50 mm. It has a main body with three parts (regions). The first part is a 30 mm long cylinder with 5 fillable rods (internal diameters of 1 mm, 2 mm, 3 mm, 4 mm, 5 mm placed at 7 mm from FOV center). This part is used to calculate the Partial Volume Effect (PVE). The different diameters of the fillable rods are used to find the activity recovery coefficients required for the spatial resolution. The second part is a 15 mm long cylinder used to evaluate the image uniformity. The third part is a 15 mm long cylinder which has two cold cylindrical chambers. One of cold cylinders is filled with water and the other with air to evaluate spill-over ratios and scatter correction. Each of the cold cylinders have 8 mm diameter by 15 mm length for spill-over ratio calculation and scatter correction performance. The third phantom used is a voxelized phantom to simulate realistic acquisition model. It is a combination of an interfile and a raw image data. These provide details on the patient data.

The phantom volumes are attached to sensitive detectors to record information or data regarding the hits (particle interaction). Two important pieces of information obtained related to hits are as follows:

- a. Compton and Rayleigh interactions occurring inside all the phantom volumes before the detection in the scanner system position of interaction
- b. The last volume in which Compton and Rayleigh interactions occurred

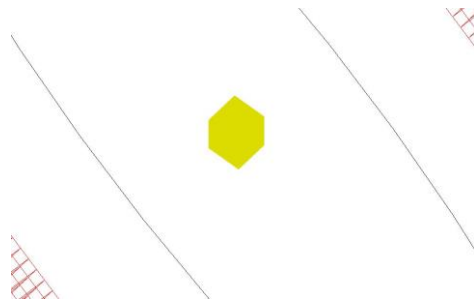


Figure 21. Simulated NEMA 4 cube phantom

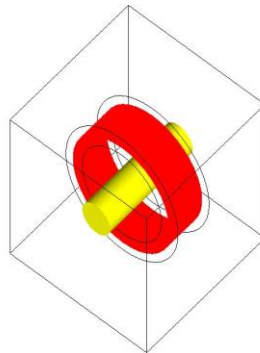


Figure 22. Simulated NEMA 2 cylindrical phantom

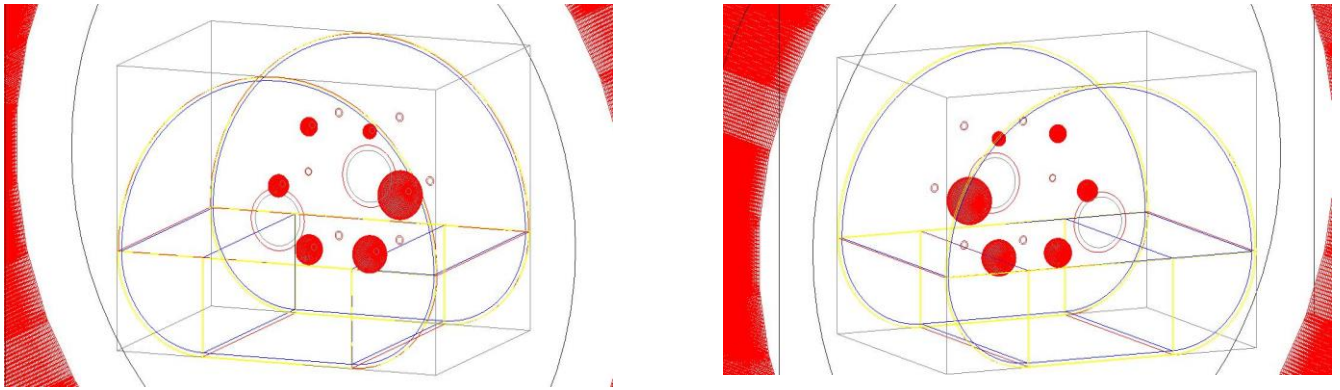


Figure 23. Simulated NEMA 2 IEC phantom (shown in different angles)

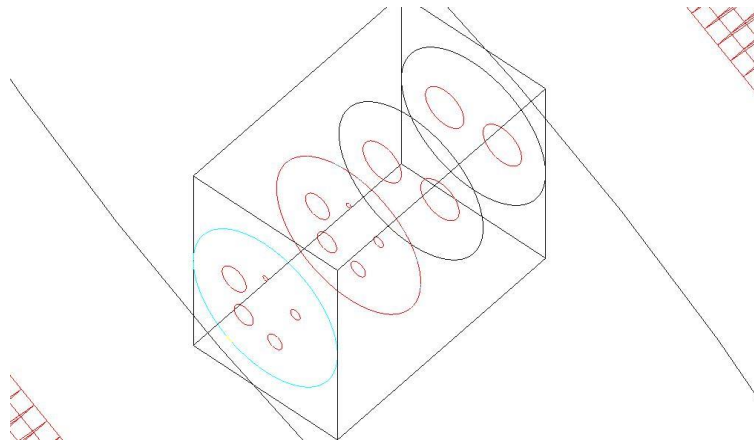


Figure 24. Simulated NEMA 4 IQ phantom

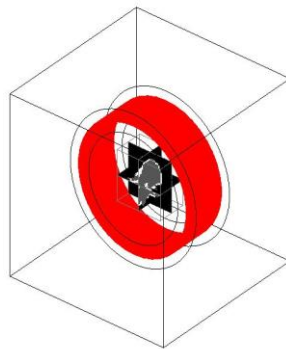


Figure 25. Simulated voxelized brain phantom

4.5 Setting-up the physics processes

The processes which define the interaction of the particle and the movement of the particle in the system are modeled as physics processes. These are defined using the physics models from the Geant4 (version 4.10.03.p01) library. The following physics models are used:

- ❖ Photoelectric effect – absorption of a photon by an atomic electron leading to the emission of the electron from the atom
- ❖ Compton scattering - photon scattering by free electrons
- ❖ Rayleigh Scattering – elastic scattering which occurs when energy of gamma photon is small compared to the ionization energy of the atom, it uses Monte Carlo method
- ❖ Ionization for positrons and electrons – transfer of energy lost by a particle to an atom when the particle passes through matter
- ❖ Bremsstrahlung for positrons and electrons – generation of electromagnetic radiation by a charged particle when it accelerates in the field of another charged particle
- ❖ Positron annihilation – annihilation of a positron with an atomic electron
- ❖ Multiple Scattering for positrons and electrons - elastic Coulomb scattering which occurs when a charged particle passes through matter

Cuts are defined in the system to have a threshold below which secondary particles cannot be generated. They are defined in terms of distance with respect to the layer level of scanner and phantom volumes. They are defined for gamma, electron and positron only.

4.6 Initialization

The cross-section tables and the boundary check for the geometry are triggered in this step. All the previous steps are called pre-initialization steps and all the next steps are called post-initialization steps. Hence, the geometry of the scanner and the phantom cannot be modified after this step. It is performed by the following command:

```
#=====
# INITIALISATION
#=====

/gate/run/initialize
```

Figure 26. Code for initialization

4.7 Digitizer definition

The particle is generated and transported through the materials of the system's volumes in GATE using by the Geant4 model. The particle is generated using parameters such as initial type, time, momentum, energy, initial position, etc. Then, the trajectory of the particle's movement during a step, between different interactions is estimated. This leads to changes in the energy and momentum of the particle which are calculated and updated. When the interactions occur in a volume attached to a sensitive detector, the

data related to the interaction of the particle called Hits (deposited energy, the momentum before and after the interaction, the name of the volume where the interaction occurred, etc.) are stored. The simulation continues till the energy of the particle falls below a threshold value defined in the model. The detected Hits are processed by the adder module to get Singles which are further processed to detect the Coincidences. The coincidence window and a paralyzable / non-paralyzable dead time are defined as per specifications in Table 4. The energy of reference is set to 511 keV for detecting the photons emitted from the positron annihilation and the energy resolution is set to 26%. The energy window (threshold value and uphold value) are defined for each system in Table 4. A noise module with Gaussian energy and Poisson inter-event time interval is defined to account for the background detection count rate due to natural radioactivity of the LSO / LYSO crystals. Multiple coincidences are rejected. To implement the time-of-flight technology, different time resolution values are considered for simulation.

4.8 Source definition

The source is the volume in which the particles are emitted. It is defined by its parameters such as activity of the source, stable or unstable state of isotope, half-life of radioisotope, particle emitted and the dimensions of the source and geometric dimensions. Fluorine-18 (F18) radioactive isotope is used as source and its half-life is 109.8 minutes or 6586 seconds. For the voxelized (brain) phantom, data for the source are from interfile and ASCII file.

4.9 Defining data output

The results of the simulation are stored in a ROOT (*.root) file. It contains all the information regarding Hits, Singles and Coincidences by enabling the respective flags.

4.10 Starting an acquisition and running the simulation

The information to define a time step and the simulation time are given for the acquisition during the simulation. The Mersenne Twister random number generator is used as it has better performance than the other random number generators. The GATE commands are written and saved in a macro file (*.mac). This file is run from the GATE prompt using the execute command. The simulation runs in time slices till the end of the acquisition time. Each time slice occurs for the given time step period. The simulation starts from 0.0 seconds and ends at the given simulation time.

Chapter 5

SIMULATION RESULTS AND PARAMETERS

5.1 Sensitivity

Sensitivity is the probability of the detection by the PET system – the ability to correctly identify the abnormal cells or lesions from the normal cells. It measures the proportion of the actual positives (true positives) correctly identified – the count per unit time for a given source activity. It is measured by moving the line source in the axial direction. Here, a Fluorine-18 spherical source of 0.3 mm diameter and activity of 5 MBq is used. It is initially placed at the center of the FOV and then moved in the axial direction. It is calculated as follows:

$$\text{Sensitivity} = (T + S - R - B) / (A \times \beta)$$

where T refers to true coincidence events, S refers to scatter coincidence events, R refers to random coincidence events, B refers to background count due to the LSO or LYSO crystals' natural radioactivity, A refers to the activity of the source and β is the branching ratio (0.967).

Table 5, Table 6 and Table 7 list the position of the source, true coincidence events, scatter coincidence events, random coincidence events, background count, sensitivity and absolute sensitivity for the Biograph Vision, HRRT, UHR PET systems respectively.

Table 5. Sensitivity for Biograph Vision PET system

Position (mm)	T (cps)	S (cps)	R (cps)	B (cps)	Sensitivity (cps/kBq)
-450	0	0	540	6	0.113
-400	0	2	709	6	0.147
-375	0	10	565	7	0.116
-350	6943	276	696	7	1.348
-175	47093	1406	886	11	9.845
-150	46850	1309	801	8	9.793
-100	47249	1189	627	8	9.887
-90	48141	1172	569	9	10.08
-80	48448	1108	546	6	10.135
-70	48895	1163	527	10	10.242
-60	49207	1141	509	9	10.306
-50	49422	1149	485	8	10.357
-40	50241	1173	444	7	10.54
-30	50944	1188	446	9	10.688
-20	51689	1209	455	7	10.845
-10	52704	1151	464	8	11.041
0	53137	1234	411	7	11.159
10	52549	1205	414	7	11.031
20	51695	1249	451	7	10.855
30	51061	1223	487	10	10.711
40	50303	1156	492	8	10.54
50	49421	1192	492	10	10.364
60	49103	1160	534	10	10.283
70	48602	1204	567	10	10.182
80	48360	1182	565	12	10.127
90	47828	1209	620	9	10.012
100	47570	1228	618	7	9.963
150	46761	1261	861	5	9.753
200	47520	1394	1070	9	9.893
350	6979	280	679	8	1.359
375	0	20	556	7	0.112
400	0	5	706	10	0.147
450	0	0	516	0	0.107

Table 6. Sensitivity for HRRT PET system

Position (mm)	T (cps)	S (cps)	R (cps)	B (cps)	Sensitivity (cps/kBq)
-475	0	1	176	8	0.038
-450	0	1	178	8	0.038
-425	0	2	239	5	0.05
-400	0	2	252	8	0.053
-350	2	6	311	12	0.065
-300	7967	685	666	8	1.65
-200	20802	1104	718	9	4.38
-150	23686	1027	565	10	4.992
-100	19365	918	570	8	4.075
-90	18736	876	572	9	3.936
-80	18188	882	560	9	3.826
-70	18332	834	559	10	3.846
-60	19384	877	517	9	4.082
-50	21404	815	498	12	4.49
-40	25311	827	437	12	5.313
-30	29164	832	373	13	6.124
-20	33424	827	372	13	7.004
-10	38497	832	309	14	8.067
0	40671	861	289	10	8.528
10	37484	840	308	13	7.86
20	33426	868	332	8	7.023
30	29405	871	378	8	6.182
40	25494	859	411	12	5.363
50	21367	849	505	4	4.49
60	19339	842	487	11	4.071
70	18111	864	544	11	3.81
80	17869	861	523	15	3.763
90	18642	886	530	9	3.927
100	19338	890	575	12	4.062
150	23387	1024	550	11	4.933
200	20765	1071	684	8	4.373
250	23630	1102	698	8	4.969
300	7963	653	612	8	1.654
350	0	6	341	5	0.07
400	0	3	262	3	0.054
425	0	0	222	6	0.047
450	0	0	182	3	0.038
475	0	0	137	7	0.03

Table 7. Sensitivity for UHR PET system

Position (mm)	T (cps)	S (cps)	R (cps)	B (cps)	Sensitivity (cps/kBq)
-400	2164	53	753	278	0.245
-350	3371	176	1413	285	0.382
-300	6947	1126	3733	308	0.834
-100	15034	645	1367	323	2.893
-90	14757	656	1354	311	2.843
-80	14512	634	1328	334	2.789
-70	14637	611	1287	316	2.822
-60	14654	607	1237	334	2.831
-50	14561	575	1196	305	2.82
-40	14534	534	1241	318	2.794
-30	14689	549	1184	301	2.844
-20	14983	552	1150	335	2.906
-10	15155	545	1187	337	2.932
0	15183	562	1133	321	2.956
10	15080	544	1143	338	2.925
20	14781	569	1128	332	2.873
30	14808	532	1190	331	2.858
40	14666	534	1235	346	2.817
50	14497	548	1208	350	2.789
60	14621	590	1275	326	2.815
70	14405	578	1279	307	2.771
80	14646	587	1332	349	2.803
90	14781	623	1352	337	2.837
100	14867	667	1388	336	2.856
300	6832	1087	3740	324	0.797
350	3326	170	1417	332	0.361
400	2214	58	792	301	0.244

From the above tables, it can be seen that the peak absolute sensitivity for Biograph Vision is 11.159 cps/kBq, HRRT is 8.528 cps/kBq and UHR is 2.956 cps/kBq. Biograph vision has a better rate of detecting true coincidences than the other two systems.

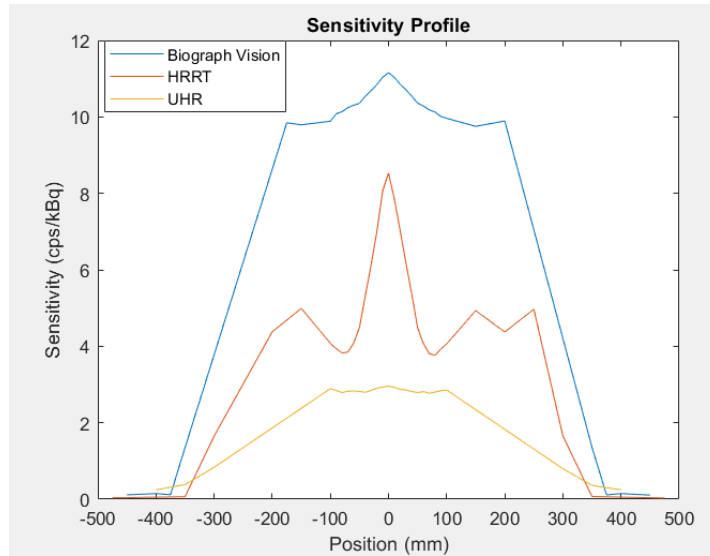


Figure 27. Sensitivity profile for Biograph Vision, HRRT and UHR PET systems

5.2 Noise Equivalent Count Rate (NECR) and Signal-to-Noise Ratio (SNR)

NECR is determined from the raw emission data obtained from the simulation. It is a good indicator of the image quality because it is the ratio of the square of the true coincidence events to the total coincidence events. It provides an estimate of the number of true coincidences in a real system in the presence of scatter and random coincidences. A Fluorine-18 source of 3.2 mm diameter and 50 mm length is used. It is placed at 45 mm from the center of the FOV. The activity of the source is initially defined as 20 MBq and changed in steps of 60 MBq till 320 MBq. NECR is linearly proportional to the

square of SNR. SNR is the measure of the actual signal to that of the noise signals and is an important factor for the image quality measurements. They are calculated as follows:

$$NECR = T^2 / (T + S + R)$$

$$SNR = \sqrt{NECR} = T / \sqrt{(T + S + R)}$$

where T refers to true coincidence events, S refers to scatter coincidence events and R refers to random coincidence events. Table 8, Table 9 and Table 10 list the activity of the source, coincidence events and NECR for the Biograph Vision, HRRT and UHR PET systems respectively.

Table 8. NECR for Biograph Vision PET system

Activity (MBq)	Total (kcps)	T (kcps)	S (kcps)	R (kcps)	NECR (kcps)	SNR
20	106.432	67.261	29.604	9.567	42.506	6.52
80	471.954	234.164	104.079	133.711	116.182	10.779
140	882.576	359.981	160.874	361.721	146.827	12.117
200	1310.851	453.983	203.337	653.531	157.227	12.539
260	1744.066	524.344	234.76	984.962	157.641	12.556
320	2170.464	575.694	257.117	1337.653	152.697	12.357

Table 9. NECR for HRRT PET system

Activity (MBq)	Total (kcps)	T (kcps)	S (kcps)	R (kcps)	NECR (kcps)	SNR
20	90.741	44.199	36.867	9.675	21.529	4.64
80	226.951	84.685	67.735	74.531	31.6	5.621
140	239.557	72.365	56.153	111.039	21.86	4.675
200	203.94	51.558	38.658	113.724	13.034	3.61
260	155.325	33.461	24.18	97.684	7.208	2.685
320	111.917	20.711	14.767	76.439	3.833	1.958

Table 10. NECR for UHR PET system

Activity (MBq)	Total (kcps)	T (kcps)	S (kcps)	R (kcps)	NECR (kcps)	SNR
20	33.738	14.505	13.182	6.051	6.236	2.497
80	201.367	56.269	51.468	93.63	15.724	3.965
140	462	95.44	87.551	279.009	19.716	4.44
200	457.132	86.972	81.392	288.768	16.547	4.068
260	474.00	64.574	59.387	350.039	8.797	2.966
320	464.00	54.007	49.642	360.351	6.286	2.507

From the above tables, it can be seen that the peak NECR for Biograph Vision is 157.641 kcps at 260 MBq, HRRT is 31.6 kcps at 80 MBq and UHR is 19.716 kcps at 140 MBq. The peak SNR is 12.556 at 260 MBq for Biograph Vision, 5.621 at 80 MBq for HRRT and 4.44 at 140 MBq for UHR. For all the systems, after the source activity with the peak NECR, the count rate performance of the systems decreases because of more scatter and random coincidences. Biograph vision has a better count rate performance and can also support a higher source activity range than the other two systems.

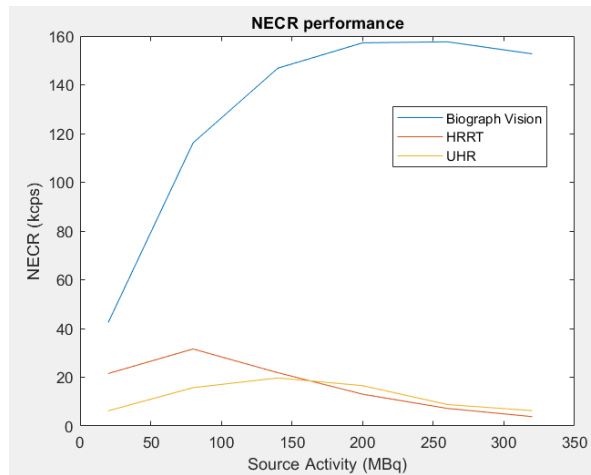


Figure 28. NECR performance for Biograph Vision, HRRT and UHR PET systems

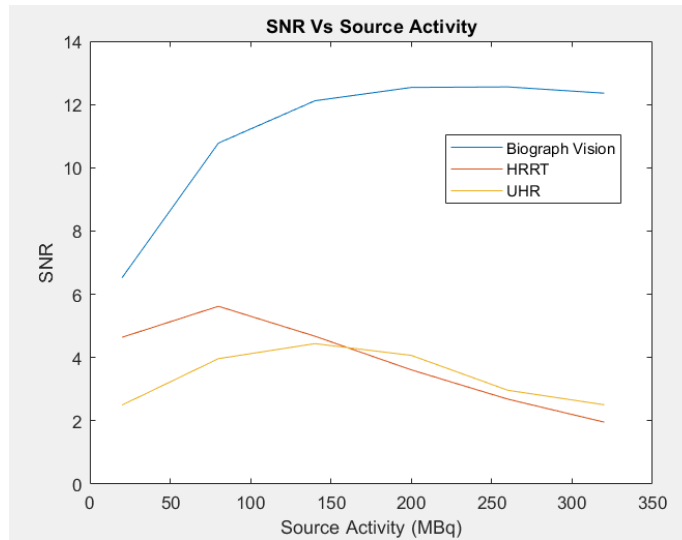


Figure 29. SNR vs source activities for Biograph Vision, HRRT and UHR PET systems

5.3 True fraction and Random fraction

The true fraction and random fraction are determined from the raw emission data obtained from the simulation. True fraction provides the rate of the true coincidence events detected and is important because the true coincidence events are the events that maintain the image quality during reconstruction. Random fraction provides the rate of the random coincidence events detected. The random coincidence events reduce the image quality during reconstruction and the random fraction provides the information required for the attenuation correction techniques. The simulation process is the same as for the NECR. They are calculated as follows:

$$\text{True Fraction (TF)} = T / (T + S + R)$$

$$\text{Random Fraction (RF)} = R / (T + S + R)$$

where T refers to true coincidence events, S refers to scatter coincidence events and R refers to random coincidence events. Table 11, Table 12 and Table 13 list the activity of the source, TF and RF for Biograph Vision, HRRT and UHR PET systems respectively.

Table 11. True fraction and random fraction for Biograph Vision PET system

Activity (MBq)	Total (kcps)	T (kcps)	S (kcps)	R (kcps)	True Fraction	Random Fraction
20	106.432	67.261	29.604	9.567	0.632	0.09
80	471.954	234.164	104.079	133.711	0.496	0.283
140	882.576	359.981	160.874	361.721	0.408	0.41
200	1310.851	453.983	203.337	653.531	0.346	0.499
260	1744.066	524.344	234.76	984.962	0.301	0.565
320	2170.464	575.694	257.117	1337.653	0.265	0.616

Table 12. True fraction and random fraction for HRRT PET system

Activity (MBq)	Total (kcps)	T (kcps)	S (kcps)	R (kcps)	True Fraction	Random Fraction
20	90.741	44.199	36.867	9.675	0.487	0.107
80	226.951	84.685	67.735	74.531	0.373	0.328
140	239.557	72.365	56.153	111.039	0.302	0.464
200	203.94	51.558	38.658	113.724	0.253	0.558
260	155.325	33.461	24.18	97.684	0.215	0.629
320	111.917	20.711	14.767	76.439	0.185	0.683

Table 13. True fraction and random fraction for UHR PET system

Activity (MBq)	Total (kcps)	T (kcps)	S (kcps)	R (kcps)	True Fraction	Random Fraction
20	33.738	14.505	13.182	6.051	0.43	0.179
80	201.367	56.269	51.468	93.63	0.279	0.465
140	462	95.44	87.551	279.009	0.207	0.604
200	457.132	86.972	81.392	288.768	0.19	0.632
260	474.00	64.574	59.387	350.039	0.136	0.738
320	464.00	54.007	49.642	360.351	0.116	0.777

From the above tables, it can be seen that the true fraction is high at 20 MBq (lower source activity) and decreases as the source activity increases for all the systems. This is because the higher source activity leads to an increase in the random coincidences being detected. Hence, the random fraction is high for the highest source activity (at 320 MBq in the simulations) and less at lower source activity (at 20 MBq in the simulations).

The highest TF for Biograph Vision is 63.196%, HRRT is 48.709% and UHR is 42.993%. The lowest RF for Biograph Vision is 8.989%, HRRT is 10.662% and UHR is 17.935%. Biograph vision has the highest TF and lowest RF when compared to the other two systems.

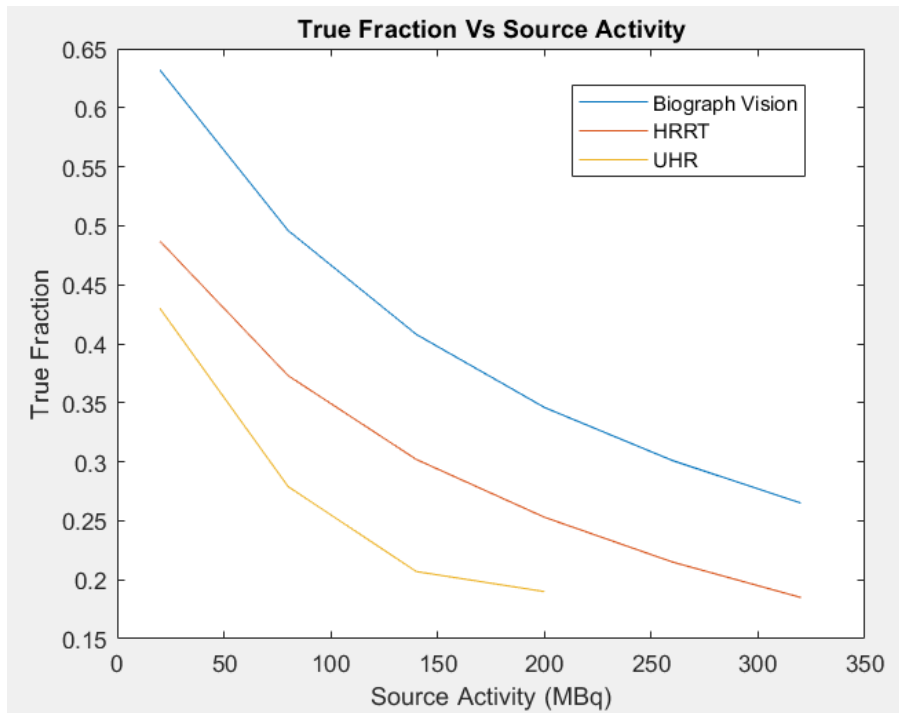


Figure 30. True Fraction for Biograph Vision, HRRT and UHR PET systems

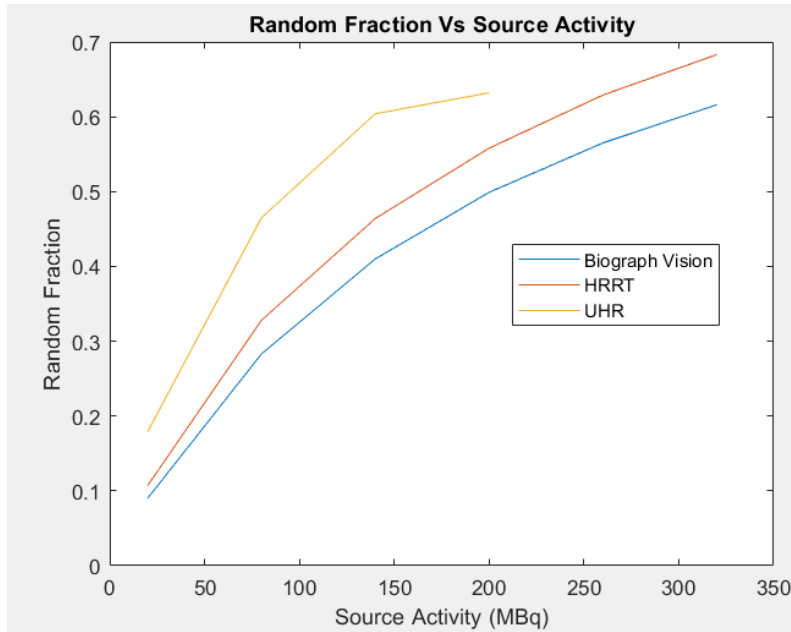


Figure 31. Random Fraction for Biograph Vision, HRRT and UHR PET systems

5.4 Scatter fraction

The scatter fraction is determined from the raw emission data obtained from the simulation. It provides the rate of the scatter coincidence events detected. As the scatter coincidence events reduce the quality of the image during reconstruction, the scatter fraction provides the information required for the scatter correction techniques. The simulation process for the process with random events is the same as for the NECR. While the NECR is a function of the source activity, scatter fraction is determined for a single source activity which renders the random events negligible. The random events are made negligible by using a source of 0.1 MBq activity. Scatter fraction is calculated as:

$$\text{Scatter Fraction (SF)} = S / (T + S)$$

where T refers to true coincidence events, S refers to scatter coincidence events and R refers to random coincidence events. Table 14 lists the true coincidence events, scatter coincidence events and scatter fraction for the Biograph Vision, HRRT and UHR PET systems.

Table 14. Scatter fraction for Biograph Vision, HRRT and UHR PET systems

System	T (cps)	S (cps)	Scatter Fraction
Biograph Vision	338	136	0.287
HRRT	290	234	0.446
UHR (250 keV - 650 keV)	153	145	0.486
UHR (450 keV - 650 keV)	12	6	0.333

From the above table, it can be seen that Biograph vision has the lowest SF when compared to the other two systems.

5.5 Time resolution and ToF gain

The time of flight is defined by using the time resolution block in GATE. The effect of the ToF is shown by plotting the total number of coincidences as function of time resolution. For the simulation, a NEMA NU 2 cylindrical phantom of 40 mm diameter by 70 mm length placed at the center of FOV is used. The source is a Fluorine-18 source of 3.2 mm diameter and 50 mm length placed at 45 mm from the center of the FOV. The activity of the source is defined as 5 MBq. Table 15, Table 16 and Table 17 list the time resolution, total number of coincidence events, true coincidence events, scatter

coincidence events, random coincidence events, NECR, SNR, true fraction and random fraction for the Biograph Vision, HRRT and UHR PET systems respectively.

Table 15. NECR and SNR with ToF for Biograph Vision PET system

Time resolution (ps)	Total (cps)	T (cps)	S (cps)	R (cps)	NECR (cps)	SNR	True Fraction	Random Fraction
20000	1773	711	843	219	285.122	16.886	0.401	0.124
15000	2262	949	1102	211	398.144	19.954	0.42	0.093
10000	3111	1376	1533	202	608.607	24.67	0.442	0.065
5000	4733	2095	2449	189	927.324	30.452	0.443	0.04
2000	5329	2378	2760	191	1061.153	32.575	0.446	0.036
1000	5320	2379	2760	181	1063.842	32.617	0.447	0.034
500	5323	2379	2760	184	1063.243	32.607	0.447	0.035
100	5321	2379	2761	181	1063.642	32.614	0.447	0.034
50	5322	2380	2761	181	1064.337	32.624	0.447	0.034
10	5321	2380	2761	180	1064.537	32.627	0.447	0.034
0	5321	2380	2761	180	1064.537	32.627	0.447	0.034

Table 16. NECR and SNR with ToF for HRRT PET system

Time resolution (ps)	Total (cps)	T (cps)	S (cps)	R (cps)	NECR (cps)	SNR	True Fraction	Random Fraction
20000	2886	715	1904	267	177.14	13.309	0.248	0.093
15000	3714	926	2524	264	230.877	15.195	0.249	0.071
10000	4949	1240	3447	262	310.689	17.626	0.251	0.053
5000	6784	1727	4806	251	439.642	20.968	0.255	0.037
2000	7106	1824	5024	258	468.193	21.638	0.257	0.036
1000	7111	1824	5025	262	467.863	21.63	0.257	0.037
500	7099	1824	5025	250	468.654	21.648	0.257	0.035
100	7103	1824	5025	254	468.39	21.642	0.257	0.036
50	7105	1824	5025	256	468.258	21.639	0.257	0.036
10	7105	1824	5025	256	468.258	21.639	0.257	0.036
0	7105	1824	5025	256	468.258	21.639	0.257	0.036

Table 17. NECR and SNR with ToF for UHR PET system

Time resolution (ps)	Total (cps)	T (cps)	S (cps)	R (cps)	NECR (cps)	SNR	True Fraction	Random Fraction
20000	1259	385	717	157	117.732	10.85	0.306	0.125
15000	1579	507	920	152	162.792	12.759	0.321	0.096
10000	2109	683	1278	148	221.19	14.872	0.324	0.07
5000	2840	948	1737	155	316.445	17.789	0.334	0.055
2000	2965	985	1830	150	327.226	18.089	0.332	0.051
1000	2964	984	1830	150	326.672	18.074	0.332	0.051
500	2963	986	1830	147	328.112	18.114	0.333	0.05
100	2961	986	1830	145	328.334	18.12	0.333	0.049
50	2961	986	1830	145	328.334	18.12	0.333	0.049
10	2961	986	1830	145	328.334	18.12	0.333	0.049
0	2961	986	1830	145	328.334	18.12	0.333	0.049

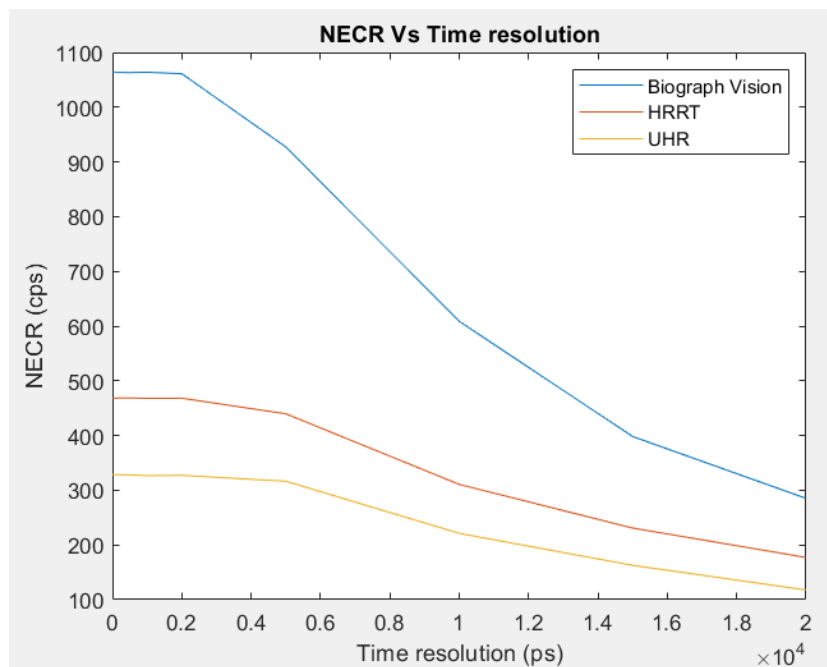


Figure 32. NECR vs time resolution for Biograph Vision, HRRT and UHR PET systems

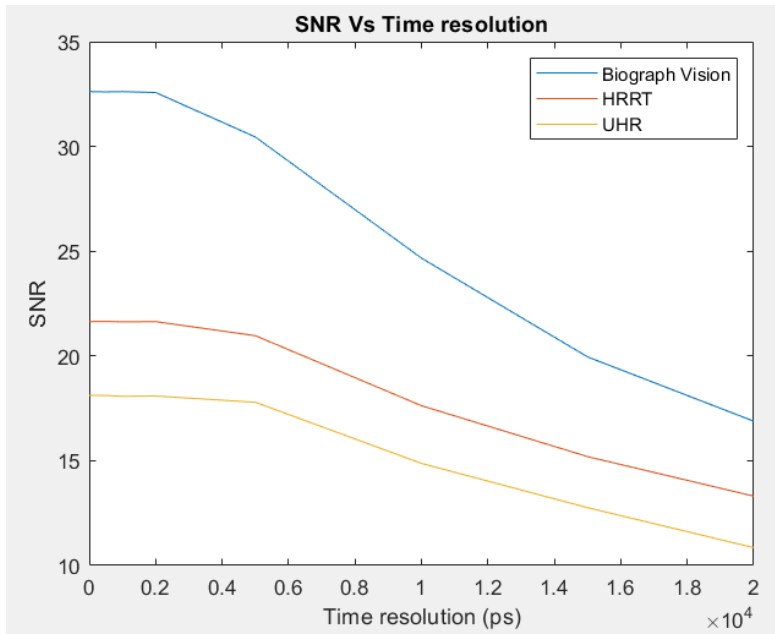


Figure 33. SNR vs time resolution for Biograph Vision, HRRT and UHR PET systems

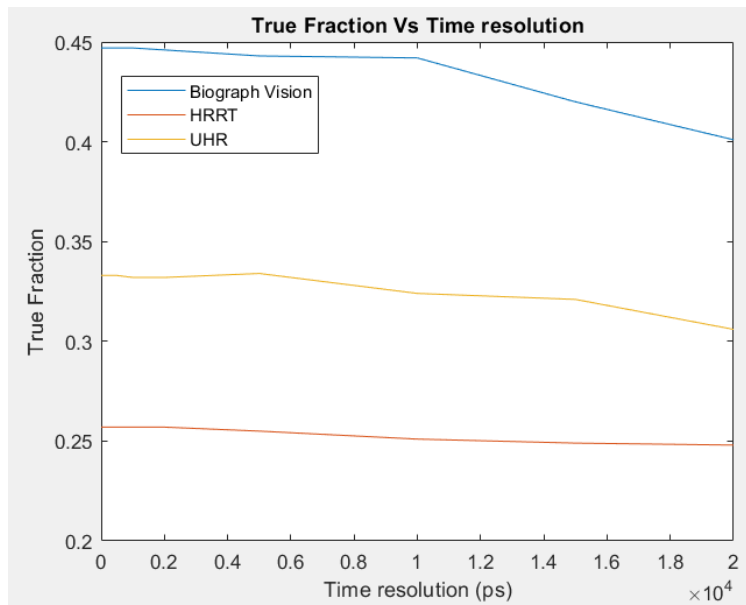


Figure 34. TF vs time resolution for Biograph Vision, HRRT and UHR PET systems

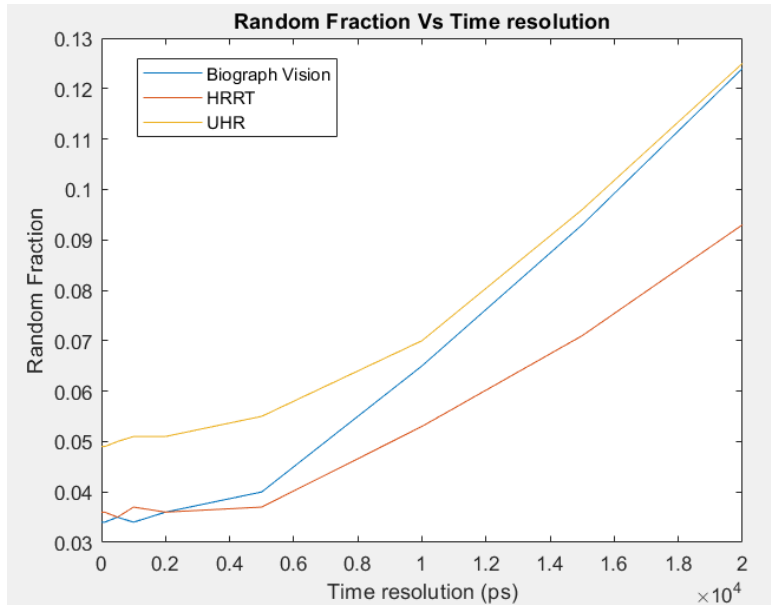


Figure 35. RF vs time resolution for Biograph Vision, HRRT and UHR PET systems

Table 18, Table 19 and Table 20 list the time resolution, true coincidence events, scatter coincidence events and scatter fraction for the Biograph Vision, HRRT and UHR PET systems respectively.

Table 18. Scatter fraction with ToF for Biograph Vision PET system

Time resolution (ps)	T (cps)	S (cps)	Scatter Fraction
20000	80	97	0.542
10000	139	163	0.534
5000	217	267	0.551
1000	247	290	0.538
100	247	290	0.537
50	247	290	0.537
10	247	290	0.537
0	247	290	0.537

Table 19. Scatter fraction with ToF for HRRT PET system

Time resolution (ps)	T (cps)	S (cps)	Scatter Fraction
20000	86	177	0.66
10000	140	361	0.718
5000	195	501	0.718
1000	204	521	0.718
100	204	521	0.718
50	204	521	0.718
10	204	521	0.718
0	204	521	0.718

Table 20. Scatter fraction with ToF for UHR PET system

Time resolution (ps)	T (cps)	S (cps)	Scatter Fraction
20000	37	77	0.675
10000	67	147	0.684
5000	95	195	0.672
1000	97	207	0.681
100	97	207	0.681
50	97	207	0.681
10	97	207	0.681
0	97	207	0.681

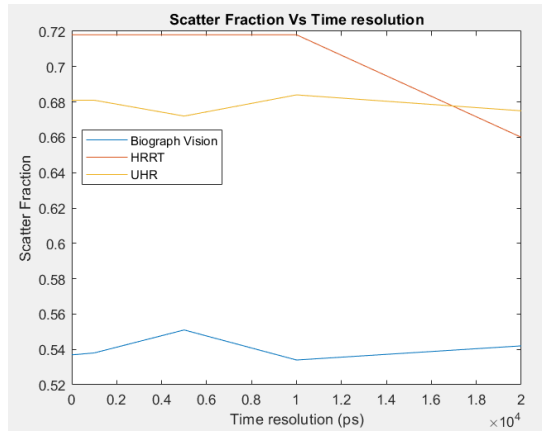


Figure 36. SF vs time resolution for Biograph Vision, HRRT and UHR PET systems

From the above tables, it can be seen that the performance of the systems increases with decrease in the time resolution value (i.e.) at lower time resolution which makes the system provide better image resolution after reconstruction at lower time resolution. The SNR for the PET systems with the time resolution is high and improved compared to the SNR of the PET systems without time resolution (as per results in section 5.2). The NECR gain (ToF gain) and the SNR gain for the image after reconstruction are important parameters to measure the image quality and calculated as below:

$$\Delta x = ((T2 - T1) \times c) / 2 = (\Delta t \times c) / 2$$

$$\text{ToF Gain (G}_{\text{ToF}}) \text{ or NECR Gain (G}_{\text{NECR}}) = D / \Delta x$$

$$\text{SNR Gain (G}_{\text{SNR}}) = \sqrt{G_{\text{NECR}}} = \sqrt{(D / \Delta x)} \approx \text{SNR}_{\text{ToF}} / \text{SNR}_{\text{Non-ToF}}$$

where D refers to patient (phantom) diameter, Δx is the location of the annihilation event along the LOR given by ToF measurement, T1 and T2 are the time at which the coincidence photons are detected, Δt is the time difference between the detection of the two coincidence photons and c is speed of light (3×10^8 m/s). Table 21 shows the calculation for the ToF gain and SNR gain with patient diameter D as 40 cm. From the below table, it can be seen that the ToF gain and SNR gain increase with decrease in time resolution (i.e.) the quality of the image is better when the time resolution is small (pico-seconds).

Table 21. ToF Gain and SNR Gain for D = 40 cm

Time resolution - Δt (ps)	Δx (cm)	G_{ToF} or G_{NECR}	G_{SNR}
20000	300	0.133	0.365
10000	150	0.267	0.516
5000	75	0.533	0.73
2000	30	1.333	1.154
1000	15	2.667	1.633
500	7.5	5.33	2.308
100	1.5	26.67	5.163
50	0.75	53.33	7.303
10	0.15	266.67	16.333

5.6 Image quality and reconstruction using CASToR

For the image quality performance of the systems, NEMA NU 2 IEC phantom, NEMA NU 4 IQ phantom and voxel phantom are used. The phantom is placed at the center of the FOV. The source is a Fluorine-18 source of 3.2 mm diameter and 50 mm length placed at the center of the FOV. The activity of the source is defined as 5 MBq. Table 22, Table 23 and Table 24 list the phantom used, coincidence events, NECR, SNR, TF and RF for the Biograph Vision, HRRT and UHR PET systems respectively.

Table 22. Image quality analysis for Biograph Vision PET system

Phantom	Total (kcps)	T (kcps)	S (kcps)	R (kcps)	NECR (kcps)	SNR	True Fraction	Random Fraction
Voxel phantom	274.53	271.824	0.821	1.888	269.145	16.406	0.99	0.007
NEMA NU 2 phantom	98.88	62.251	34.343	2.281	39.191	6.26	0.63	0.023
NEMA NU 4 phantom	23.66	18.256	5.396	0.005	14.086	3.753	0.772	0

Table 23. Image quality analysis for HRRT PET system

Phantom	Total (kcps)	T (kcps)	S (kcps)	R (kcps)	NECR (kcps)	SNR	True Fraction	Random Fraction
Voxel phantom	16.41	10.155	6.253	0.003	6.284	2.507	0.619	0
NEMA NU 2 phantom	162.75	96.947	62.559	3.242	57.749	7.599	0.596	0.02
NEMA NU 4 phantom	419.22	416.041	1.136	2.041	412.886	20.32	0.992	0.005

Table 24. Image quality analysis for UHR PET system

Phantom	Total (kcps)	T (kcps)	S (kcps)	R (kcps)	NECR (kcps)	SNR	True Fraction	Random Fraction
Voxel phantom	7.34	4.959	2.381	0.002	3.35	1.83	0.675	0
NEMA NU 2 phantom	23.31	10.794	11.543	0.969	4.998	2.236	0.463	0.042
NEMA NU 4 phantom	32.02	31.012	0.158	0.853	30.036	5.481	0.968	0.027

The ROOT ^[25] output file from the GATE simulation is analyzed for the hits, singles and coincidences, and is given as input to CASToR ^[26] to first generate the data binary file (.Cdf) and data header (.Cdh) files using the castor-GATERootToCastor command as below:

castor-GATERootToCastor -i <Path and ROOT File> -o <Path and Output File> -m <Path and Macro File> -geo -s <Geometry file>

The -i represents the input file to CASToR (.root file), -o represents output file generated by CASToR (.Cdf and .Cdh files), -m represents GATE macro file (.mac file), -geo represents instruction to generate CASToR geometry file (.geom file and is stored in the path config/scanner) from the given GATE macro file and -s represents the scanner used to acquire the data as input to CASToR (.geom file).

The generated data files from the above command are given as input to the castor-recon command for the reconstruction of the image as below. The reconstructed images are stored in the specified output folder.

```
castor-recon -df <.Cdh file> -opti <optimization algorithm> -it <no. of iterations>:<no. of subsets> -proj <projector name> -conv <convolution kernel> -dim <dimension> -dout <output folder>
```

The castor-recon commands used for reconstruction of the image for each of the system are as below. The reconstruction is done for the voxelized brain phantom.

```
castor-recon -df PET_bgvsn_voxel_df.Cdh -opti MLEM -it 30:16 -proj joseph -conv gaussian,4.,4.5,3.5::psf -dim 32,32,16 -dout PET_bgvsn_recon_voxel
```

```
castor-recon -df PET_hrtr_voxel_df.Cdh -opti MLEM -it 30:16 -proj joseph -conv gaussian,4.,4.5,3.5::psf -dim 32,32,16 -dout PET_hrtr_recon_voxel
```

```
castor-recon -df PET_uhr_voxel_df.Cdh -opti MLEM -it 30:16 -proj joseph -conv gaussian,4.,4.5,3.5::psf -dim 32,32,16 -dout PET_uhr_recon_voxel
```

A 3D gaussian kernel of 4 mm trans-axial FWHM, 4.5 mm axial FWHM with 3.5 sigmas in the kernel is used for obtaining a spatially uniform image-based PSF. The reconstructed images are given the dimension of 32 x 32 x 16 based on the input interfile (example from GATE). Iterative MLEM optimization algorithm is used to obtain an optimal reconstructed image and the projector used is based on Joseph's method. The output files from the castor-recon command are interfile data (.hdr files) and raw data (.img files). These files are given as input to the AMIDE tool for rendering the 3D image view of the phantom.



Figure 37. Reconstructed image (transverse – left, coronal – middle, sagittal - right) for Biograph Vision
PET



Figure 38. Reconstructed image (transverse – left, coronal – middle, sagittal - right) for HRRT PET



Figure 39. Reconstructed image (transverse – left, coronal – middle, sagittal - right) for UHR PET

The following images shown the enlarged view of the reconstructed images to view the images at the pixel level.

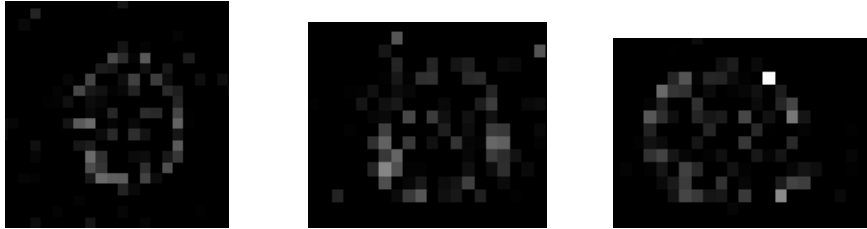


Figure 40. Pixelated image (transverse – left, coronal – middle, sagittal - right) for Biograph Vision PET



Figure 41. Pixelated image (transverse – left, coronal – middle, sagittal - right) for HRRT PET



Figure 42. Pixelated image (transverse – left, coronal – middle, sagittal - right) for UHR

From the above images, it can be seen that UHR PET systems has a better pixel resolution while the other two PET systems are blurred at the pixel level.

Chapter 6

CONCLUSION AND FUTURE WORK

6.1 Conclusion

The modeling of PET system in GATE has made significant impact in the evaluation of the performance and image reconstruction capabilities of the systems. It also provides a framework for the analysis and assessment of correction techniques and their accuracy. The three-dimensional simulation modeling of the PET systems provides a realistic view, explicit simulation and scintillation process, and detailed understanding of the systems. It provides an accurate (within few percent discrepancy) information on the coincidences, line of response, energy deposited, dose concentration, count rate performance, sensitivity, spatial resolution, etc. of the model. The usage of Geant4 commands and library for the model provides a greater chance of obtaining a precise model of the systems. The usage of OpenGL library for visualization helps provide more insight of the real systems and the operation. The usage of Monte Carlo methods helps in optimization of the data and improve the accuracy of the analysis as it is based on random processes.

The state-of-the-art PET systems are faced with compromise on either spatial resolution or the performance. To avoid this, models with better spatial resolution and performance are being modeled and analyzed.

The biograph vision PET system was introduced for its excellent sensitivity and time resolution. The HRRT PET system is dedicated for human brain study. It has high sensitivity, better spatial resolution and accuracy in localizing the molecular interactions in the brain. The UHR PET system provides a truly pixelated detectors in the system based on the LabPET-II technology. It had better spatial resolution and resolving capability.

Most of the research consisted of learning and understanding GATE software, how to model the systems and perform the simulation by the study of extensive documentation of GATE, research papers and benchmark tutorials with examples. The compressed usage of Geant4 code in GATE to suit only for the emission tomography modelling makes it easier for the users not to study the whole Geant4 geometries and physics models. The Geant4 library support for physics models has a huge advantage that the users do not have to design the complex models and particle propagation in the system and can use a small set of codes from the library for the simulation. Also, handling the time-dependent nature of the particle propagation in time frames or slices and using the Monte Carlo method is a special and attractive feature of GATE. The computational time can be reduced by using voxelized phantoms and sources as it reduces the pre-calculation time for the next volume / boundary during tracking.

The usage of ROOT and CASToR softwares for the analysis of the simulation output from GATE provides an easy platform and accurate results of the simulation. These softwares support the GATE output files and the users are provided with documentation on the specific usage for GATE related analysis. The clear and neat conversion of the output files from GATE by CASToR to generate its inputs files makes it very flexible and easy to use to retrieve information on the number of prompts, true, scatter and random coincidences. Also, the castor-recon command is a special feature which helps the users to reconstruct the image from the GATE output (ROOT-meta data file) with the necessary kernels, optimization algorithm and projectors.

In this research, the three PET systems (Biograph Vision, HRRT and UHR) were analyzed for their physical (Sensitivity, NECR, SNR, TF, RF, SF and time resolution) performance and image reconstruction performance. Among these, Biograph Vision provides a better physical performance because of its mini-block arrangement of crystals attached to detector block (provides a high packing fraction for the scanner system) compared to the other two systems while UHR provides a better image reconstruction performance due to its pixelated detectors.

6.2 Future Prospects

The research was made by using the cylindrical PET scanner system and few restrictions such as multiple coincidence rejections in GATE. The following can be done to have a better accuracy, analyze the spatial resolution and better image reconstruction capabilities of the system:

- Usage of ECAT scanner system for further analysis - It provides the sinogram output which supports spatial resolution and image reconstruction capability analysis specifically
- Analyzing the systems by including multiple coincidences – using multiple coincidence sorters in the PET system
- Analyzing with highest energy coincidence sorters – to increase the sensitivity and NECR
- Analyzing the system with delayed coincidence module

. Also, more detailed study on reconstruction of the image using CASToR software (castor-recon command, projector methods, kernels) and AMIDE tool would help in obtaining a better reconstructed image from the simulations.

REFERENCES

- [1] M. Pizzichemi, “Positron Emission Tomography: state of the art and future developments”, in “2016 Journal of Instrumentation (JINST) 11”, C08004 (2016).
- [2] Kara Duncan, “Radiopharmaceuticals in PET Imaging”, in “1998 J Nucl Med Techno”, vol 26, pp 228-234 (1998).
- [3] “Positron Emission Tomography”, URL https://www.radioactivity.eu.com/site/pages/Positron_emission_tomography.htm (Accessed: 2020-03-25)
- [4] J. Cal-González, J. L. Herraiz, S. España, M. Desco, J. J. Vaquero and J. M. Udías., “Positron range estimations with PeneloPET”, in “2013 Physics in Medicine and Biology”, vol 58 (15):5127-5152 (2013).
- [5] Pizzichemi M1, Stringhini G, Niknejad T, Liu Z, Lecoq P, Tavernier S, Varela J, Paganoni M, Auffray E., “A new method for depth of interaction determination in PET detectors.” in “2016 Physics in Medicine and Biology”, vol 61 (12):4679-4698 (2016).
- [6] G. Stringhini et al, “Development and evaluation of a practical method to measure the Depth of Interaction function for a single side readout PET detector”, in “2016 Journal of Instrumentation (JINST) 11”, P11014 (2016).
- [7] Lipeng Pan, J. He and Lei Ma, “An initial simulation study of PET imaging by GATE”, in “2010 The 2nd International Conference on Information Science and Engineering, Hangzhou”, pp. 1-4 (2010).
- [8] C. J. Groiselle, H. A. Kudrolli and S. J. Glick, “Monte-Carlo simulation of the photodetection systems prototype PET scanner using GATE: a validation study”, in “2004 IEEE Symposium Conference Record Nuclear Science, Rome”, pp. 3130-3132 (2004).
- [9] Agostinelli S. et al., “Medical Applications of the Geant4 Toolkit”, in “2001 Advanced Monte Carlo for Radiation Physics, Particle Transport Simulation and Applications, Springer, Berlin, Heidelberg”, pp 543-548 (2001).
- [10] S. Jan et al., “GATE: A simulation toolkit for PET and SPECT”, in “2004 Phys Med Biol”, vol 49, pp. 4543-4561 (2004).

- [11] S. Jan, C. Comtat, D. Strul, G. Santin and R. Trebossen, “Monte Carlo Simulation for the ECAT EXACT HR+ system using GATE”, in “2005 IEEE Transactions on Nuclear Science”, vol. 52, no. 3, pp. 627-633, (2005).
- [12] “ROOT Web Page”, URL <http://root.cern.ch> (Accessed: 2020-03-25)
- [13] “STIR Web Page”, URL <http://stir.sourceforge.net/> (Accessed: 2020-03-25)
- [14] Thibaut Merlin, Simon Stute, et al., “CASToR: a generic data organization and processing code framework for multi-modal and multi-dimensional tomographic reconstruction”, in “2018 Physics in Medicine & Biology”, vol 63 (18)5505 (2018).
- [15] “CASToR Web Page”, URL <http://www.castor-project.org/> (Accessed: 2020-03-25)
- [16] “Monte Carlo Methods Web Page”, URL http://www.ibfm.cnr.it/mcet/Background/MC_methods/mc_methods.html (Accessed: 2020-03-25)
- [17] “Geant4 Web Page”, URL <https://geant4.web.cern.ch/> (Accessed: 2020-03-25)
- [18] S. Jan et al., “*GATE - Geant4 Application for Tomographic Emission: a simulation toolkit for PET and SPECT Web Page*”, URL <https://www.ncbi.nlm.nih.gov/pmc/articles/PMC3267383/> (Accessed: 2020-03-25)
- [19] “GATE Web Page”, URL <http://www.opengatecollaboration.org/> (Accessed: 2020-03-25)
- [20] C. C. Yang, J. Seidel, Y. Wang, J. S. Lee, M. G. Pomper and B. M. W. Tsui, “Validation of GATE Monte Carlo simulation of the performance characteristics of a GE eXplore VISTA small animal PET system”, in “2007 IEEE Nuclear Science Symposium Conference Record, Honolulu, HI”, pp. 3187-3190 (2007).
- [21] D. Guez, F. Bataille, C. Comtat, P. Honore, S. Jan and S. Kerhoas, “Counting Rates Modeling for PET Scanners With GATE”, in “2008 IEEE Transactions on Nuclear Science”, vol. 55, no. 1, pp. 516-523 (2008).
- [22] “AMIDE Web Page”, URL <http://amide.sourceforge.net/> (Accessed: 2020-03-25)
- [23] É. Gaudin, M. Toussaint, C. Thibaudeau, M. Paillé, R. Fontaine and R. Lecomte, “Performance Simulation of an Ultrahigh Resolution Brain PET Scanner Using 1.2-mm Pixel Detectors”, in “2019 IEEE Transactions on Radiation and Plasma Medical Sciences”, vol. 3, no. 3, pp. 334-342 (2019).

[24] *GATE Users Guide V8.0*, GATE, version 8.0 (2017).

[25] *ROOT manual for GATE users*, ROOT, version 1.1 (2018).

[26] *Customizable and Advanced Software for Tomographic Reconstruction (CASToR) General Documentation*", CASToR, version 2.1 (2019).

[27] "Wikipedia Web Page", URL <https://www.wikipedia.org/> (Accessed: 2020-03-25)